Extended Hartree-Fock study of the single-particle potential: The nuclear symmetry energy, nucleon effective mass, and folding model of the nucleon optical potential

Doan Thi Loan,[1] Bui Minh Loc,[1,2] and Dao T. Khoa[1,*]

[1]*Institute for Nuclear Science and Technology, VINATOM, 179 Hoang Quoc Viet, Cau Giay, Hanoi, Vietnam*

[2]*University of Pedagogy, Ho Chi Minh City, Vietnam*

(Received 8 July 2015; revised manuscript received 20 August 2015; published 4 September 2015)

The nucleon mean-field potential has been thoroughly investigated in an extended Hartree-Fock (HF) calculation of nuclear matter (NM) using the CDM3Y3 and CDM3Y6 density dependent versions of the M3Y interaction. The single-particle (SP) energies of nucleons in NM are determined according to the Hugenholtz–Van Hove theorem, which gives rise naturally to a rearrangement term (RT) of the SP potential at the Fermi momentum. Using the RT obtained exactly at the different NM densities and neutron-proton asymmetries, a consistent method is suggested to take into account effectively the momentum dependence of the RT of the SP potential within the standard HF scheme. To obtain a realistic momentum dependence of the nucleon optical potential (OP), the high-momentum part of the SP potential was accurately readjusted to reproduce the observed energy dependence of the nucleon OP over a wide range of energies. The impact of the RT and momentum dependence of the SP potential on the density dependence of the nuclear symmetry energy and nucleon effective mass has been studied in detail. The high-momentum tail of the SP potential was found to have a sizable effect on the slope of the symmetry energy and the neutron-proton effective mass splitting at supranuclear densities of the NM. Based on a local density approximation, the folding model of the nucleon OP of finite nuclei has been extended to take into account consistently the RT and momentum dependence of the nucleon OP in the same mean-field manner, and successfully applied to study the elastic neutron scattering on the lead target at the energies around the Fermi energy.

DOI: 10.1103/PhysRevC.92.034304 PACS number(s): 21.65.Cd, 21.65.Mn

I. INTRODUCTION

The nucleon mean-field potential or single-particle (SP) potential is the most important quantity determining the SP properties of neutrons and protons in the nuclear matter (NM) as well as in the finite nuclei [1], and it has been the focus of recent many-body studies of the NM, like the Brueckner-Hartree-Fock (BHF) calculations of the NM starting from a realistic choice of the free nucleon-nucleon (NN) interaction [2–4] or the mean-field studies of the NM on the Hartree-Fock (HF) level, using the different versions of the effective (in-medium) NN interaction [5–7]. A quite interesting aspect of the SP potential is its direct connection with the nuclear symmetry energy [4,7], a key quantity necessary for the determination of the equation of state (EOS) of the asymmetric NM [8]. Many microscopic studies of the EOS were done based either on the nonrelativistic or relativistic mean-field potential given by realistic two-body and three-body NN forces or interaction Lagrangians [9,10]. Such microscopic many-body studies did show the important role played by the Pauli blocking effects as well as the increasing strength of the higher-order NN correlations at the high NM densities. These medium effects are usually considered as the main physics origin of an explicit density dependence embedded in the different versions of the effective NN interaction, being used currently in the HF calculations of the nuclear structure or nuclear reaction studies. Among them, quite popular are the density dependent versions of the M3Y interaction (originally constructed to reproduce the G-matrix elements of the Reid [11] and Paris [12] NN potentials in an oscillator basis), which have been successfully used in the HF studies of the NM [13–17] as well as in the folding model studies of the nucleon-nucleus and nucleus-nucleus scattering [18–23].

With the phenomenological density dependence of the M3Y interaction parametrized to give a realistic description of the NM saturation properties [13,14,18] within the HF frame, the HF nucleon optical potential (or the high-momentum part of the SP potential) was used to determine the explicit energy dependence of the density dependent M3Y interaction [13,24] based on the observed energy dependence of the nucleon optical potential (OP). These density and energy dependent versions of the M3Y interaction have been further used in the folding model calculation of the nucleon-nucleus and nucleus-nucleus OP [19–22]. The simple assumption for the SP potential in the NM made in Refs. [13,24] is roughly equivalent to the microscopic SP potential of the Brueckner-Bethe theory [25], which lacks the so-called *rearrangement* term that arises naturally in the Landau theory for the infinite Fermi systems [26]. Such a rearrangement term (RT) also appears when the SP potential is evaluated from the total NM energy using the Hugenholtz and Van Hove (HVH) theorem [27], which is exact for all the interacting Fermi systems, independent of the type of the interaction between fermions. For the infinite NM, it is straightforward to see that the HVH theorem is satisfied on the HF level only when the in-medium NN interaction is density independent, i.e., when the RT is equal to zero [28]. It is, therefore, of high interest to assess the impact of the RT on the SP potential in a mean-field study of the NM within the standard HF frame using a realistic density dependent NN interaction. Moreover, given the fact that the nuclear symmetry energy and nucleon effective mass

*khoa@vinatom.gov.vn

are directly linked to the momentum and density dependence of the single-nucleon potential [4,7], it is highly desirable to have a method to take into account properly the density and momentum dependence of the RT of the SP potential on the HF level, which is the main motivation of the present study. It is further expected that, in a local density approximation, one should be able to include, in the same mean-field manner, the RT and momentum dependence of the density dependent NN interaction into the folding model calculation of the nucleon OP for the finite nuclei, which is being evaluated so far mostly on the HF level [19,20,22,23]. Towards this goal, an extension of the single-folding approach for the nucleon OP [19] has been done and applied to study the elastic neutron scattering on the lead target measured at the incident energies of 30.4 and 40 MeV [29].

II. EXTENDED HF FORMALISM FOR THE SINGLE-PARTICLE POTENTIAL

In the present HF approach, we consider the homogeneous, spin-saturated NM of given neutron (ρ_n) and proton (ρ_p) densities, or equivalently, of given total nucleon density $\rho = \rho_n + \rho_p$ and neutron-proton (NP) asymmetry $\delta = (\rho_n - \rho_p)/\rho$. Using the direct ($v_c^{\rm D}$) and exchange ($v_c^{\rm EX}$) parts of the (central) in-medium NN interaction v_c, the total NM energy can be determined in the standard nonrelativistic HF scheme as $E = E_{\rm kin} + E_{\rm pot}$, where the kinetic and potential energies are

$$E_{\rm kin} = \sum_{k\sigma\tau} n_\tau(k)\frac{\hbar^2k^2}{2m_\tau}, \tag{1}$$

$$\begin{aligned} E_{\rm pot} &= \frac{1}{2}\sum_{k\sigma\tau}\sum_{k'\sigma'\tau'} n_\tau(k)n_{\tau'}(k')\big[\langle \boldsymbol{k}\sigma\tau,\boldsymbol{k}'\sigma'\tau'|v_c^{\rm D}|\boldsymbol{k}\sigma\tau,\boldsymbol{k}'\sigma'\tau'\rangle \\ &\quad + \langle \boldsymbol{k}\sigma\tau,\boldsymbol{k}'\sigma'\tau'|v_c^{\rm EX}|\boldsymbol{k}'\sigma\tau,\boldsymbol{k}\sigma'\tau'\rangle\big], \\ &= \frac{1}{2}\sum_{k\sigma\tau}\sum_{k'\sigma'\tau'} n_\tau(k)n_{\tau'}(k')\langle \boldsymbol{k}\sigma\tau,\boldsymbol{k}'\sigma'\tau'|v_c|\boldsymbol{k}\sigma\tau,\boldsymbol{k}'\sigma'\tau'\rangle_{\mathcal{A}}. \end{aligned} \tag{2}$$

The SP wave function $|\boldsymbol{k}\sigma\tau\rangle$ is plane wave, and the summation in Eqs. (1) and (2) is done separately over the neutron ($\tau = n$) and proton ($\tau = p$) SP indices. The nucleon momentum distribution $n_\tau(k)$ in the spin-saturated NM is a step function determined with the Fermi momentum $k_F^{(\tau)} = (3\pi^2\rho_\tau)^{1/3}$ as

$$n_\tau(k) = \begin{cases} 1 & \text{if} \quad k \leqslant k_F^{(\tau)}, \\ 0 & \text{otherwise.} \end{cases} \tag{3}$$

According to the Landau theory for the infinite Fermi systems [25,26], the SP energy $e_\tau(k)$ in the NM is determined as

$$e_\tau(k) = \frac{\partial E}{\partial n_\tau(k)} = t_\tau(k) + U_\tau(k) = \frac{\hbar^2k^2}{2m_\tau} + U_\tau(k), \tag{4}$$

which is the change of the NM energy caused by the removal or addition of a nucleon with the momentum k. The single-nucleon potential $U_\tau(k)$ consists of both the HF and rearrangement terms

$$U_\tau(k) = U_\tau^{\rm (HF)}(k) + U_\tau^{\rm (RT)}(k), \tag{5}$$

$$\text{where} \quad U_\tau^{\rm (HF)}(k) = \sum_{k'\sigma'\tau'} n_{\tau'}(k')\langle \boldsymbol{k}\sigma\tau,\boldsymbol{k}'\sigma'\tau'|v_c|\boldsymbol{k}\sigma\tau,\boldsymbol{k}'\sigma'\tau'\rangle_{\mathcal{A}} \tag{6}$$

$$\begin{aligned} \text{and} \quad U_\tau^{\rm (RT)}(k) &= \frac{1}{2}\sum_{k_1\sigma_1\tau_1}\sum_{k_2\sigma_2\tau_2} n_{\tau_1}(k_1)n_{\tau_2}(k_2) \\ &\quad \times \langle \boldsymbol{k}_1\sigma_1\tau_1,\boldsymbol{k}_2\sigma_2\tau_2|\frac{\partial v_c}{\partial n_\tau(k)}|\boldsymbol{k}_1\sigma_1\tau_1,\boldsymbol{k}_2\sigma_2\tau_2\rangle_{\mathcal{A}}. \end{aligned} \tag{7}$$

When the nucleon momentum approaches the Fermi momentum ($k \to k_F^{(\tau)}$), $e_\tau(k_F^{(\tau)})$ determined from Eqs. (4)–(7) is exactly the Fermi energy given by the Hugenholtz–Van Hove theorem [27]. Using the transformation [28]

$$\left.\frac{\partial}{\partial n_\tau(k)}\right|_{k\to k_F^{(\tau)}} = \frac{\partial\rho_\tau}{\partial n_\tau\big(k_F^{(\tau)}\big)}\frac{\partial k_F^{(\tau)}}{\partial\rho_\tau}\frac{\partial}{\partial k_F^{(\tau)}} = \frac{1}{\Omega}\frac{\pi^2}{\big[k_F^{(\tau)}\big]^2}\frac{\partial}{\partial k_F^{(\tau)}}, \tag{8}$$

where Ω is the total volume of the NM in the momentum space, the rearrangement term of the SP potential U_τ at the Fermi momentum can be obtained [30] as

$$\begin{aligned} U_\tau^{\rm (RT)}\big(k\to k_F^{(\tau)}\big) &= 4\frac{\pi^2}{\big[k_F^{(\tau)}\big]^2}\sum_{\tau_1\tau_2}\frac{\Omega}{2(2\pi)^6}\iint n_{\tau_1}(k_1)n_{\tau_2}(k_2) \\ &\quad \times \langle \boldsymbol{k}_1\tau_1,\boldsymbol{k}_2\tau_2|\frac{\partial v_c}{\partial k_F^{(\tau)}}|\boldsymbol{k}_1\tau_1,\boldsymbol{k}_2\tau_2\rangle_{\mathcal{A}}d^3k_1d^3k_2. \end{aligned} \tag{9}$$

At variance with the RT part, the HF part of the SP potential can be readily evaluated at any momentum

$$U_\tau^{\rm (HF)}(k) = 2\sum_{\tau'}\frac{\Omega}{(2\pi)^3}\int n_{\tau'}(k')\langle \boldsymbol{k},\boldsymbol{k}'\tau'|v_c|\boldsymbol{k},\boldsymbol{k}'\tau'\rangle_{\mathcal{A}}d^3k'. \tag{10}$$

The spin components of plane waves in the HF and RT parts of the SP potential are averaged out, and this results in the spin degeneracy factors 4 and 2 in the expressions (9) and (10), respectively. We keep in mind that the SP potential is determined consistently at each total NM density ρ. As a result, U_τ is a function of the total NM density ρ, the neutron-proton asymmetry δ, and the nucleon momentum k. For the spin-saturated NM, only the spin-independent terms of the central NN interaction are needed for the determination of the SP potentials (9) and (10). In the present work, we have used two density dependent versions (CDM3Y3 and CDM3Y6) [18] of the M3Y interaction based on the G-matrix elements of the Paris NN potential in a oscillator basis [12]. Thus, the central part of the CDM3Yn interaction was used in the present HF calculation explicitly as

$$\begin{aligned} &v_c^{\rm D(EX)}(s) = F_0(\rho)v_{00}^{\rm D(EX)}(s) + F_1(\rho)v_{01}^{\rm D(EX)}(s)\boldsymbol{\tau}_1\cdot\boldsymbol{\tau}_2, \\ &\text{where} \quad s = |\boldsymbol{r}_1 - \boldsymbol{r}_2|. \end{aligned} \tag{11}$$

TABLE I. Parameters of the density dependence (13) of the CDM3Yn interaction. The incompressibility K of the symmetric NM, the nuclear symmetry energy S_0, and its slope L were obtained from the HF results (30) at the saturation density $\rho_0 \approx 0.17$ fm^{-3}.

Interaction i	C_i	α_i	β_i (fm^3)	γ_i (fm^3)	K (MeV)	S_0 (MeV)	L (MeV)
CDM3Y3	0 0.2985	3.4528	2.6388	−1.500	218		
	1 0.2343	7.6514	9.7494	6.6317		30.1	49.6
CDM3Y6	0 0.2658	3.8033	1.4099	−4.000	252		
	1 0.2313	7.6800	9.6498	6.7202		30.1	49.7

The radial parts $v_{00(01)}^{\mathrm{D(EX)}}(s)$ are kept unchanged as determined from the M3Y-Paris interaction [12], in terms of three Yukawas,

$$v_{00(01)}^{\mathrm{D(EX)}}(s) = \sum_{\nu=1}^{3} Y_{00(01)}^{\mathrm{D(EX)}}(\nu)\frac{\exp(-R_\nu s)}{R_\nu s}, \qquad (12)$$

and the explicit Yukawa strengths and ranges can be found, e.g., in Table I of Ref. [20]. The density dependence of the interaction (11) is assumed to have the same functional form as that introduced first in Ref. [18],

$$F_{0(1)}(\rho) = C_{0(1)}[1 + \alpha_{0(1)}\exp(-\beta_{0(1)}\rho) + \gamma_{0(1)}\rho]. \qquad (13)$$

The parameters of the *isoscalar* (IS) density dependence $F_0(\rho)$ were determined [18] to reproduce the saturation properties of the symmetric NM and give the nuclear incompressibility $K = 218$ and 252 MeV with the CDM3Y3 and CDM3Y6 interactions, respectively. These interactions, especially the CDM3Y6 version, have been well tested in numerous folding model analyses of the elastic nucleon-nucleus [19] and nucleus-nucleus scattering [21], and the charge-exchange scattering to the isobar analog states [20,23]. Like in Ref. [20], the parameters of the *isovector* (IV) density dependence $F_1(\rho)$ were determined in the present work to reproduce the BHF results for the IV term of the microscopic nucleon OP in the asymmetric NM obtained by Jeukenne, Lejeune, and Mahaux (JLM) [31,32]. Because of the RT included in the extended HF calculation of the nucleon OP, the parameters obtained for the IV density dependence $F_1(\rho)$ are slightly different from those used earlier [20,23]. For convenience of the readers who are interested in using the CDM3Yn interaction in the HF or folding model calculation, the parameters of the density dependence are given explicitly in Table I.

The HF results for the total energy per particle E/A of the asymmetric NM are shown in Fig. 1. One can see that the saturation density rapidly decreases with the increasing NP asymmetry, and the pure neutron matter ($\delta = 1$) is unbound by the (in-medium) NN interaction. At the high NM densities, the E/A curves obtained with the CDM3Y6 interaction are stiffer than those obtained with the CDM3Y3 interaction, and this is due to the higher nuclear incompressibility K given by the CDM3Y6 interaction. The behavior of the EOS of the asymmetric NM with the increasing NP asymmetries shown in Fig. 1 is typical and similar to those observed earlier in the HF calculations of the NM using the different types of the in-medium (density dependent) NN interaction [15–17].

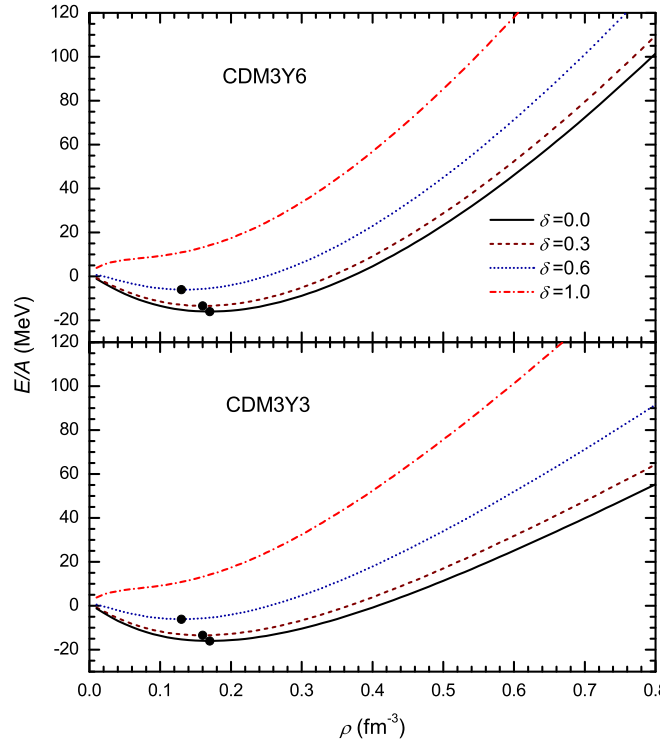

FIG. 1. (Color online) Total NM energy per particle E/A at the different NP asymmetries δ given by the HF calculation (1) and (2), using the CDM3Y3 (lower panel) and CDM3Y6 (upper panel) interactions with their IV density dependence anew determined in the present work. The solid circles are the saturation densities of the NM at the different NP asymmetries.

Given the parametrization (11) of the CDM3Y3 and CDM3Y6 interactions, the HF part of the SP potential can be explicitly obtained in terms of the IS and IV parts as

$$U_\tau^{(\mathrm{HF})}(\rho,\delta,k) = F_0(\rho)U_0^{(\mathrm{M3Y})}(\rho,k) \pm F_1(\rho)U_1^{(\mathrm{M3Y})}(\rho,\delta,k),$$

$$\text{where } U_0^{(\mathrm{M3Y})}(\rho,k) = \rho J_0^{\mathrm{D}} + \int A_0(r)v_{00}^{\mathrm{EX}}(r)j_0(kr)d^3r, \qquad (14)$$

$$\text{and } U_1^{(\mathrm{M3Y})}(\rho,\delta,k) = \rho J_1^{\mathrm{D}}\delta + \int A_1(r)v_{01}^{\mathrm{EX}}(r)j_0(kr)d^3r.$$

$$\text{Here } A_{0(1)}(r) = \rho_n \hat{j}_1\left(k_F^{(n)}r\right) \pm \rho_p \hat{j}_1\left(k_F^{(p)}r\right),$$

$$J_{0(1)}^{\mathrm{D}} = \int v_{00(01)}^{\mathrm{D}}(r)d^3r, \qquad (15)$$

$$\text{and } \hat{j}_1(x) = 3j_1(x)/x = 3(\sin x - x\cos x)/x^3.$$

The (−) sign on the right-hand side of Eq. (14) pertains to the single-proton ($\tau = p$) and (+) sign to the single-neutron ($\tau = n$) potentials. Because the original M3Y interaction is momentum independent, the momentum dependence of the HF potential (14) is entirely determined by the exchange terms of $U_{0(1)}^{(\mathrm{M3Y})}$.

Applying the HVH theorem, the RT of the SP potential is also obtained explicitly in terms of the IS and IV parts, but at

the Fermi momentum only,

$$U_\tau^{(\mathrm{RT})}\left(\rho,\delta,k_F^{(\tau)}\right)=U_0^{(\mathrm{RT})}\left(\rho,k_F^{(\tau)}\right)+U_1^{(\mathrm{RT})}\left(\rho,\delta,k_F^{(\tau)}\right),$$
$$\text{where } U_0^{(\mathrm{RT})}\left(\rho,k_F^{(\tau)}\right)=\frac{1}{2}\frac{\partial F_0(\rho)}{\partial\rho}\left[\rho^2 J_0^{\mathrm{D}}+\int A_0^2(r)v_{00}^{\mathrm{EX}}(r)d^3r\right]$$
$$\text{and } U_1^{(\mathrm{RT})}\left(\rho,\delta,k_F^{(\tau)}\right)=\frac{1}{2}\frac{\partial F_1(\rho)}{\partial\rho}\left[\rho^2 J_1^{\mathrm{D}}\delta^2+\int A_1^2(r)v_{01}^{\mathrm{EX}}(r)d^3r\right]. \tag{16}$$

One can see from Eq. (16) that the RT becomes zero if the density independent M3Y interaction is used in the HF calculation of the SP potential. In such a case, the HVH theorem is satisfied already on the HF level [28]. At a given NP asymmetry δ, the IV part of the RT is the same for both the single-neutron ($\tau=n$) and single-proton ($\tau=p$) potentials, and that affects the simple representation of the nucleon OP by Lane [33,34], where the IV parts of the neutron and proton OP are equal but with the *opposite* sign.

In general, as seen from Eq. (7), the RT of the SP potential should be present at the arbitrary nucleon momenta. Microscopically, the momentum dependence of the RT was shown, in the BHF calculation of the NM [1,3,4], to be due to the higher-order NN correlation, like the second-order diagram in the perturbative expansion of the mass operator or the contribution from the three-body forces, etc. In the finite nuclei, the rearrangement effects in the nucleon removal reactions (which have about the same physics origin as the RT potential considered here) were shown [35] to be strongly dependent on the energy of the stripping reaction, a clear indication of the momentum dependence of the RT potential. The question now is whether one can assess the momentum dependence of the RT of the SP potential on the HF level. Making use of the factorized density dependence of the CDM3Y3 and CDM3Y6 interactions, we suggest in the present work a rather simple method to include consistently a momentum dependent RT into the SP potential in the same HF framework. An important constraint of this procedure is that adding a realistic momentum dependent RT to the HF potential should improve the agreement of the calculated nucleon OP in the NM with the empirical data. It has been shown [13,24] that the momentum dependence of the HF potential (14) could account fairly well for the observed energy dependence of the nucleon OP after a slight adjustment of the interaction strength at the high energies. Therefore, we adopt phenomenologically a momentum dependent RT of the SP potential in the functional form similar to (14) as

$$U_\tau^{(\mathrm{RT})}(\rho,\delta,k)=\Delta F_0(\rho)U_0^{(\mathrm{M3Y})}(\rho,k)+\Delta F_1(\rho,\delta)U_1^{(\mathrm{M3Y})}(\rho,\delta,k), \tag{17}$$

where the (momentum-independent) rearrangement contributions to the IS and IV density dependencies of the CDM3Yn interactions are determined consistently from the exact expression (16) of the RT at the Fermi momentum as

$$\Delta F_0(\rho)=\frac{U_0^{(\mathrm{RT})}\left(\rho,k_F^{(\tau)}\right)}{U_0^{(\mathrm{M3Y})}\left(\rho,k\to k_F^{(\tau)}\right)}\quad\text{and}\quad \Delta F_1(\rho,\delta)=\frac{U_1^{(\mathrm{RT})}\left(\rho,\delta,k_F^{(\tau)}\right)}{U_1^{(\mathrm{M3Y})}\left(\rho,\delta,k\to k_F^{(\tau)}\right)}. \tag{18}$$

Consequently, the total SP potential is determined in the present HF approach as

$$\begin{aligned}U_\tau(\rho,\delta,k)&=U_0(\rho,k)\pm U_1(\rho,\delta,k)\\&=[F_0(\rho)+\Delta F_0(\rho)]U_0^{(\mathrm{M3Y})}(\rho,k)\\&\pm[F_1(\rho)\pm\Delta F_1(\rho,\delta)]U_1^{(\mathrm{M3Y})}(\rho,\delta,k),\end{aligned} \tag{19}$$

where the $(-)$ sign pertains to $\tau=p$ and the $(+)$ sign to $\tau=n$. Thus, the momentum dependence of the total SP potential U_τ is determined by that of the exchange terms of $U_{0(1)}^{(\mathrm{M3Y})}$. Due to the presence of the RT, the absolute strength of the IV term of the single-proton potential is not equal to that of the single-neutron potential. One can see from expressions (17)–(19) that the rearrangement effects actually result in a modification of the IS and IV density dependence of the central interaction (11), $v_c\to v_c+\Delta v_c$, so that the total SP potential can be estimated in the standard HF scheme as

$$U_\tau(\rho,\delta,k)=\sum_{k'\sigma'\tau'}n_{\tau'}(k')\langle\boldsymbol{k}\sigma\tau,\boldsymbol{k}'\sigma'\tau'|v_c+\Delta v_c|\boldsymbol{k}\sigma\tau,\boldsymbol{k}'\sigma'\tau'\rangle_{\mathcal{A}}. \tag{20}$$

Nucleon OP in the NM and the SP potential at high momenta

In the NM limit, the nucleon OP is determined as the (mean-field) interaction potential between the nucleon incident on the NM at a given energy E and the bound nucleons in the filled Fermi sea [24]. In general, the nucleon OP contains both the IS and IV parts [33,34] like the total SP potential (19). Given a strong dominance of the IS term of the nucleon OP [19,22], one needs first to explore the IS term of the nucleon OP predicted by the HF calculation of the NM. Applying a *continuous* choice for the nucleon SP potential [36] at the positive energies E, we obtain in the HF scheme the nucleon OP in the *symmetric* NM [13,24] as

$$\begin{aligned}U_0(\rho,E)&=U_{\mathrm{IS}}^{(\mathrm{HF})}(\rho,E)\\&=F_0(\rho)\rho\left[J_0^D+\int\hat{j}_1(k_Fr)j_0(k(E,\rho)r)v_{00}^{\mathrm{EX}}(r)d^3r\right].\end{aligned} \tag{21}$$

Here $k(E,\rho)$ is the (energy dependent) momentum of the incident nucleon propagating in the mean field of the nucleons bound in the NM, and is determined as

$$k(E,\rho)=\sqrt{\frac{2m}{\hbar^2}[E-U_0(\rho,E)]},\quad\text{with } E>0. \tag{22}$$

It is easy to see that $k(E,\rho)>k_F$ and $U_{\mathrm{IS}}^{(\mathrm{HF})}$ is just the high momentum part of the isoscalar term of the HF potential (14). Based on the above discussion, the total nucleon OP in the NM

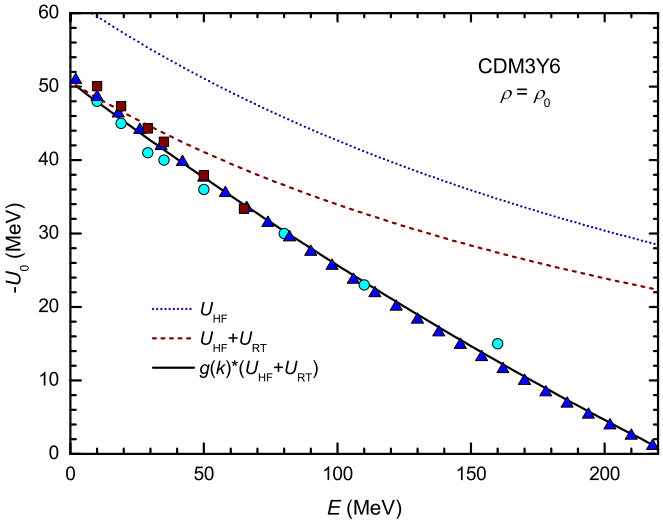

FIG. 2. (Color online) Energy dependence of the nucleon OP in the symmetric NM (evaluated at the saturation density ρ_0 with and without the RT using the CDM3Y6 interaction) in comparison with the empirical data taken from Refs. [37] (circles), [38] (squares), and [39] (triangles). The momentum dependent factor $g(k)$ has been iteratively adjusted to the best agreement of the calculated nucleon OP (24) with the empirical data (solid line).

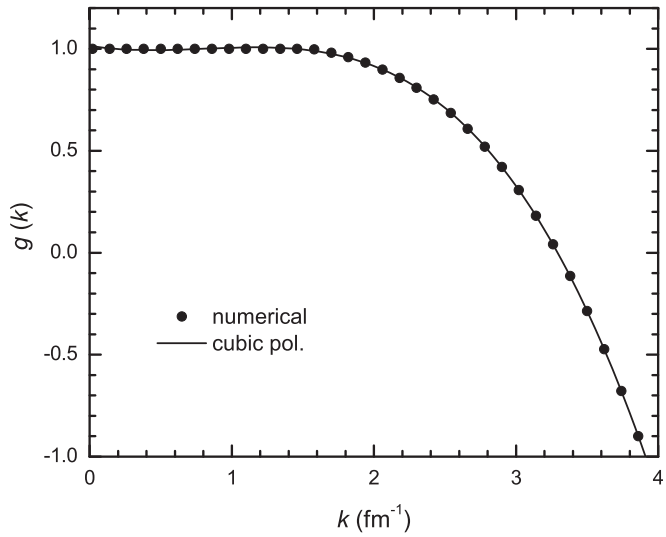

FIG. 3. Momentum dependent scaling factor $g(k)$ obtained with both the CDM3Y3 and CDM3Y6 interactions from the best (HF+RT) fit of the nucleon OP (24) to the empirical energy dependence of the nucleon OP [39]. The points are the numerical results that are well reproduced by a cubic polynomial (solid line).

should also have a contribution from the RT added,

$$U_0(\rho,E) = U_{\rm IS}^{\rm (HF)}(\rho,E) + U_{\rm IS}^{\rm (RT)}(\rho,E) = [F_0(\rho) + \Delta F_0(\rho)]U_0^{\rm (M3Y)}(\rho,k(E,\rho)), \quad (23)$$

where the density dependence $\Delta F_0(\rho)$ of the RT is determined by relation (18).

The total nucleon OP (23) evaluated at the saturation density ρ_0 of the symmetric NM using the CDM3Y6 interaction are compared with the empirical data [37–39] in Fig. 2. Although the inclusion of the RT significantly improved the agreement of the calculated U_0 with the data at the lowest energies, it remains somewhat more attractive at the higher energies in comparison with the empirical trend. Such an effect is easily understood in light of the microscopic BHF results for the nucleon OP [36], where the energy dependence was shown to come not only from the exchange part, but also from the direct part of the microscopic OP because of the energy dependence of the Brueckner G matrix. That is the reason why a slight linear energy dependence has been introduced into the CDM3Y6 interaction [18,19], in terms of the $g(E)$ factor. To be consistent with the momentum dependence of the SP potential under study, instead of the $g(E)$ factor, we scale in the present work the CDM3Yn interaction (11) by a momentum dependent function $g(k(E,\rho))$, and iteratively adjust its strength to the best agreement of the (HF+RT) nucleon OP obtained at the saturation density ρ_0 with the empirical data, as shown in Fig. 2. As a result,

$$U_0(\rho,E) = g(k(E,\rho))[F_0(\rho) + \Delta F_0(\rho)]U_0^{\rm (M3Y)}(\rho,k(E,\rho)), \quad (24)$$

where $k(E,\rho)$ is determined self-consistently from $U_0(E,\rho)$ by Eq. (22). At variance with the $g(E)$ factor fixed by the incident energy [18,19], $g(k(E,\rho))$ is now a momentum dependent function (see Fig. 3), carrying the important signature of the momentum dependence of the nucleon mean-field potential. Numerically, the obtained $g(k)$ function is nearly identical for both the CDM3Y3 and CDM3Y6 interactions, and it can be considered as the explicit momentum dependence of the CDM3Yn interaction that allows the incident nucleon to feel the nucleon mean-field potential during its interaction with the nucleons bound in the NM. In this sense, such a momentum dependence is of a similar nature as the momentum dependence of the G matrix in the microscopic BHF study of NM, which is determined self-consistently through the momentum dependence of the SP energies embedded in the denominator of the Bethe-Goldstone equation [2,3]. The technical difference here is that the k dependence of $g(k)$ has been determined from the best fit of the calculated SP potential (24) at positive energies with the observed energy dependence of the nucleon OP. It can be seen in Fig. 3 that $g(k)$ becomes smaller unity at $k \gtrsim 1.6\,{\rm fm}^{-1}$ only. Consequently, the obtained $g(k)$ function is used further in the extended HF calculation to adjust the high-momentum part of the (HF+RT) SP potential.

The situation is quite different concerning the IV term of the nucleon OP because there are no systematic (energy dependent) empirical data available, like those discussed above for the IS potential. However, it is well established from numerous optical model analyses of the elastic nucleon scattering that the absolute strength of the IV term of the nucleon OP is much weaker than that of the IS [19,20,38], and the energy dependence of the nucleon OP is dominantly determined by that of the IS term [38]. Consequently, the momentum dependent function $g(k)$ determined above for the IS part should be a reasonable approximation for the IV part

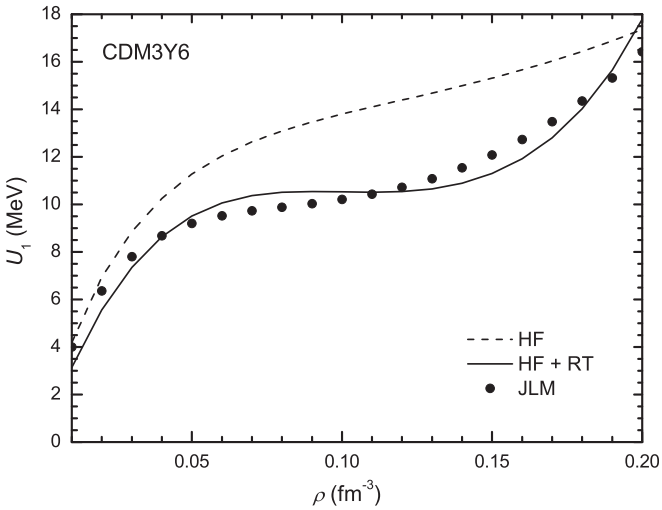

FIG. 4. Density dependence of the IV part of the neutron OP in the pure neutron matter at the energy $E = 1$ MeV, evaluated with and without the RT. The parameters (13) of the IV density dependence $F_1(\rho)$ of the CDM3Y6 interaction have been iteratively adjusted to give the best agreement of the HF+RT result with that of the BHF calculation by the JLM group (solid circles) [31,32].

of the nucleon OP in the HF+RT calculation,

$$U_1(\rho,\delta,E) = g(k(E,\delta,\rho))[F_1(\rho) + \Delta F_1(\rho,\delta)]U_1^{(\mathrm{M3Y})}(\rho,\delta,k(E,\delta,\rho)), \quad (25)$$

where $k(E,\delta,\rho)$ is determined self-consistently from the total nucleon OP in the asymmetric NM as

$$k(E,\delta,\rho) = \sqrt{\frac{2m}{\hbar^2}[E - U_0(\rho,E) \mp U_1(\rho,\delta,E)]}. \quad (26)$$

Thus, the NN interaction in the $\tau.\tau$ channel of the central force (11) is also influenced by the nucleon mean-field potential through the momentum dependent $g(k)$ function. Like in Refs. [20,23], parameters of the IV density dependence $F_1(\rho)$ of the M3Y-Paris interaction have been iteratively adjusted in the HF+RT calculation to achieve a good agreement of the IV potential (25) with the microscopic nucleon OP in the asymmetric NM given by the BHF calculation done by the JLM group [31,32], with the contribution of the RT properly included [40]. At variance with the previous studies where $F_1(\rho)$ has been determined separately at each considered energy [20,23], we have used in the present work a unique set of the parameters of $F_1(\rho)$ which were determined from the best fit of the IV potential (25) to the corresponding JLM results at the lowest energies [32], where $g(k) \approx 1$ (see Fig. 4). Together with the IS density dependence $F_0(\rho)$ determined earlier [18], the newly determined IV density dependence $F_1(\rho)$ of the CDM3Yn interactions have been used in the present work to calculate the total NM energy and the single-nucleon potential. The absolute strength of $F_1(\rho)$ in the extended HF calculation was scaled by a factor of 1.3, which was found necessary in the folding model analysis of the (p,n) scattering to the isobar analog states [20]. As a result, the nuclear symmetry energy $S(\rho_0)$ at the saturation density given by the present HF

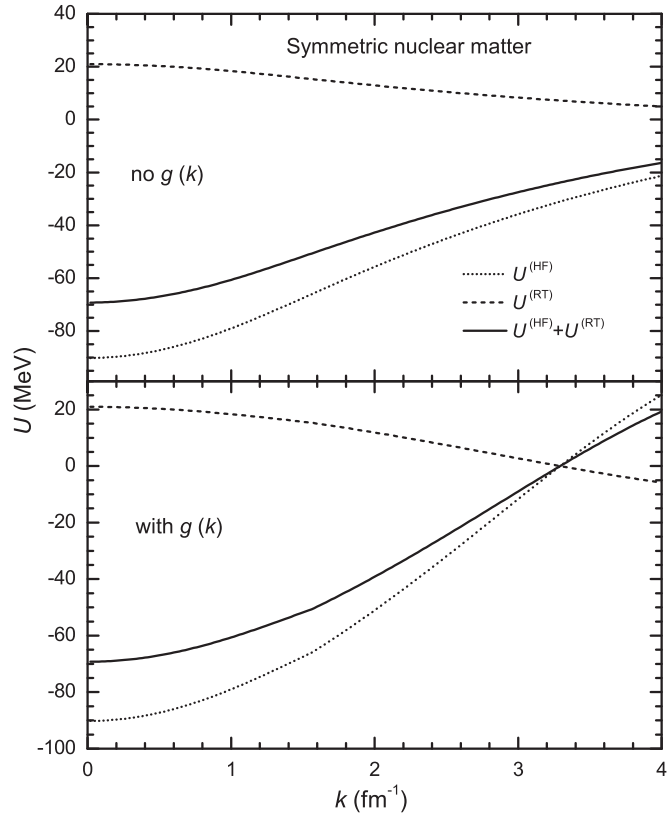

FIG. 5. Momentum dependence of the total SP potential in the symmetric NM at the saturation density ρ_0, with the explicit contributions from the RT and HF parts. The upper panel shows the results of the extended HF calculation (23), and the lower panel shows the total SP potential (24), with the high-momentum part corrected by the $g(k)$ function determined from the observed energy dependence of the nucleon OP.

calculation is very close to the empirical value of about 30 MeV (see also the next section). The final values of the parameters of $F_0(\rho)$ and $F_1(\rho)$ are given with the most important NM properties in Table I.

The total (density and momentum dependent) SP potential is now determined as

$$U_\tau(\rho,\delta,k) = g(k)[U_0(\rho,k) \pm U_1(\rho,\delta,k)], \quad (27)$$

where $U_0(\rho,k)$ and $U_1(\rho,\delta,k)$ are determined by using Eq. (19) and the same function $g(k)$ as that shown in Fig. 3. The total SP potentials obtained at the saturation density $\rho_0 \approx 0.17$ fm^{-3} from the extended HF calculation (20) of the symmetric NM and the pure neutron matter using the CDM3Y6 interaction are shown in Figs. 5 and 6, respectively. One can see that the RT is largest at the nucleon momenta close to zero, which correspond to nucleons deeply bound in the NM ($k \ll k_F$). The RT steadily decreases with the increasing nucleon momentum, and the decrease of the RT becomes faster when the high-momentum part of the SP potential is scaled by the $g(k)$ function determined [see Eqs. (24) and (25)] to reproduce the observed energy dependence of the nucleon OP. In this case, the SP potential reaches zero and changes sign at the momentum $k \approx 3.3$ fm^{-1} that corresponds to the nucleon OP

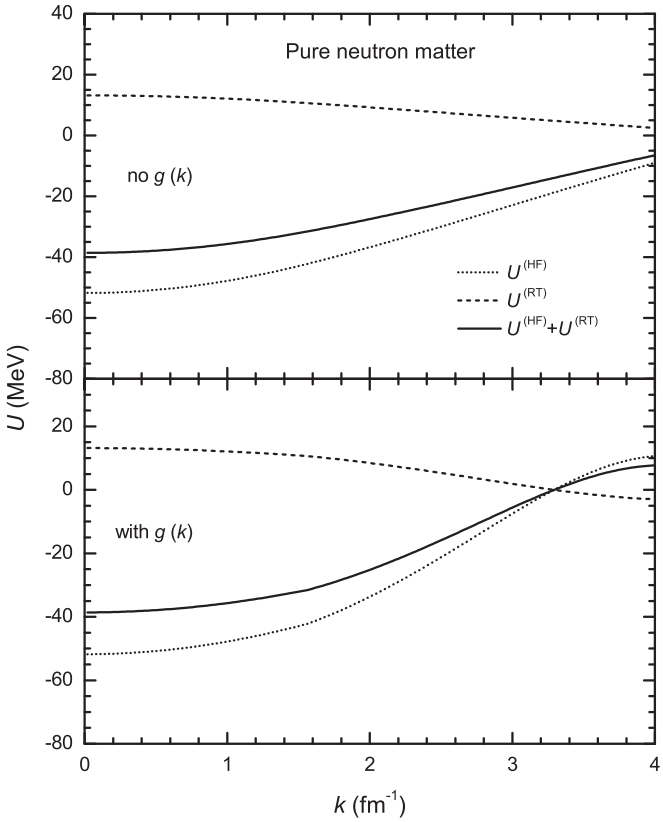

FIG. 6. The same as Fig. 5 but for the total SP potential in the pure neutron matter.

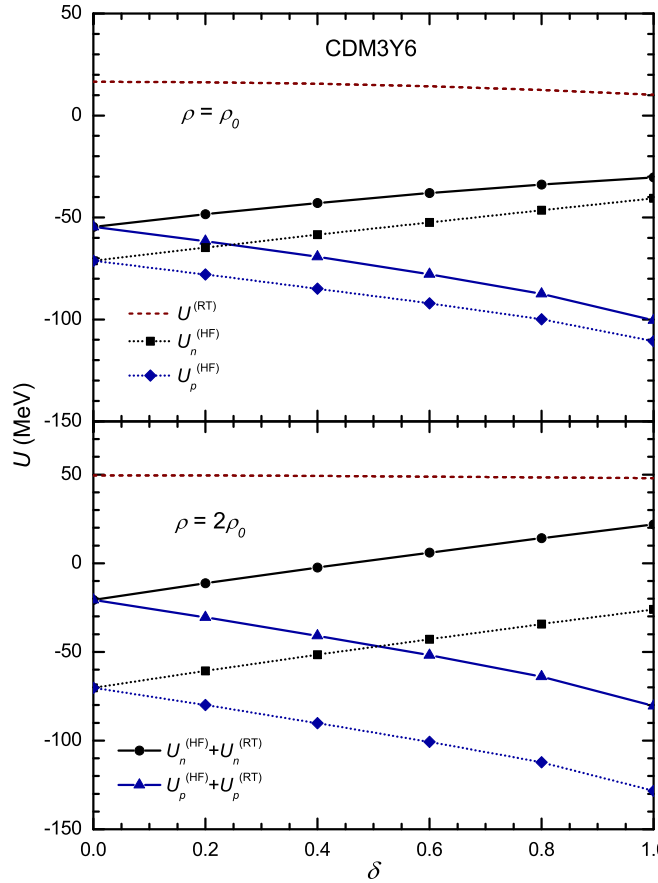

FIG. 7. (Color online) Contributions of the RT and HF parts to the total neutron and proton SP potentials evaluated at the different NP asymmetries δ and nucleon momenta $k = k_F^{(\tau)}$, using the CDM3Y6 interaction. The results obtained at the saturation density $\rho = \rho_0$ are shown in the upper panel, and those obtained at the density $\rho = 2\rho_0$ are shown in the lower panel.

at the incident energy around 220 MeV, where the empirical (Schrödinger-equivalent) $U_{\rm op}$ was shown to become repulsive [39]. Such a momentum dependence of the SP potential agrees well with that predicted by the microscopic BHF calculation (see, e.g., Figs. 6 and 7 of Ref. [3]). A decrease of the RT with the increasing nucleon momentum (or energy) also agrees with the observed energy dependence of the rearrangement effect in the nucleon removal reactions [35]. In the relative strength, the RT contributes to about 20–30% of the total strength of the SP potential at $\rho = \rho_0$ over a wide range of the nucleon momentum and is, therefore, a very clear manifestation of the HVH theorem [27].

The dependence of the neutron and proton SP potentials on the NP asymmetry (with the explicit contributions from the RT and HF parts) is shown in Fig. 7, and one can see that the RT is the same for both the neutron and proton SP potentials. In the present extended HF scheme, such an equality is exactly obtained from the RT given by the HVH theorem (16). At a given NM density, the RT decreases slightly with the increasing NP asymmetry δ. As can be seen from the lower panel of Fig. 7, the repulsive contribution of the RT becomes much stronger at the high density $\rho = 2\rho_0$, with the relative strength up to 70% of the HF term. Such a behavior of the RT is well expected, given the higher-order NN correlations and the three-body forces as the physics origin of the RT [1,3], which become much more substantial with the increasing NM density. The results of our extended HF calculation shown in Fig. 7 also agree well with those of the recent BHF calculation of the asymmetric NM by Vidaña [41], using the Argonne NN interaction (V18 version [42] with the Urbana three-body force).

To conclude this section, a simple and consistent method has been developed to account effectively for the momentum dependence of the RT of the SP potential in an extended HF calculation using the CDM3Yn density dependent interactions (11), based on the exact expression of the RT given by the HVH theorem at each NM density and the empirical energy dependence of the nucleon OP observed over a wide range of energies.

III. SINGLE-NUCLEON POTENTIAL AND THE SYMMETRY ENERGY

Given the importance of the nuclear symmetry energy for the nuclear astrophysics studies, especially, its vital role in the determination of the EOS of the asymmetric NM [8,9], we focus in the present section on the connection of the SP potential in the NM with the nuclear symmetry energy, which has been widely discussed in Refs. [4,7]. The nuclear symmetry energy $S(\rho)$ is normally defined with an expansion of the total NM energy per particle over the NP asymmetry

δ as

$$\frac{E}{A}(\rho,\delta) = \frac{E}{A}(\rho,\delta=0) + S(\rho)\delta^2 + O(\delta^4) + \cdots . \quad (28)$$

For $\delta < 1$, the contribution of $O(\delta^4)$ and the higher-order terms in Eq. (28) was proven to be quite small [3,15] and can be neglected (the so-called *parabolic* approximation). For the pure neutron matter ($\delta = 1$) the convergence of the series (28) is slower, and the parabolic law becomes less accurate. Therefore, a more general definition of the nuclear symmetry energy as the energy required per particle to change the symmetric NM into the pure neutron matter is also used in the mean-field studies,

$$S(\rho) = \frac{E}{A}(\rho,\delta=1) - \frac{E}{A}(\rho,\delta=0). \quad (29)$$

The nuclear symmetry energy $S(\rho)$ can also be expanded [43] around ρ_0 as

$$S(\rho) = S_0 + \frac{L}{3}\left(\frac{\rho-\rho_0}{\rho_0}\right) + \frac{K_{\rm sym}}{18}\left(\frac{\rho-\rho_0}{\rho_0}\right)^2 + \cdots , \quad (30)$$

where L and $K_{\rm sym}$ are the slope and curvature parameters of the symmetry energy at ρ_0. While the curvature parameter $K_{\rm sym}$ is still poorly known, it has been shown recently by Li and Han [44] that quite a robust constraint for both S_0 and L values has been established based on several tens analyses of the terrestrial nuclear physics experiments and astrophysical observations, which give $S_0 \approx 31.6 \pm 2.7$ MeV and $L \approx 58.9 \pm 16.0$ MeV. With the parameters of the IV density dependence of the CDM3Yn interaction anew determined in the present work, the values of $S_0 \approx 30.1$ MeV and $L \approx 49.7$ MeV given by the HF calculation are well within this empirical range.

Applying the HVH theorem to calculate the neutron and proton energies (4) at the corresponding Fermi momenta, one obtains [4,7] the nuclear symmetry energy directly from the difference between the neutron and proton Fermi energies as

$$t_n\left(k_F^{(n)}\right) - t_p\left(k_F^{(p)}\right) + U_n\left(\rho,\delta,k_F^{(n)}\right) - U_p\left(\rho,\delta,k_F^{(p)}\right) = 4S(\rho)\delta + O(\delta^3) + \cdots . \quad (31)$$

Thus, Eq. (31) is simply the parabolic law in the SP energy representation. As discussed in Sec. II, at given ρ and δ values the contribution of the RT to the SP potential (16) is the same for both the neutron and proton SP potentials. Therefore, the RT contribution to the nuclear symmetry energy $S(\rho)$ through the difference between the neutron and proton SP potentials in Eq. (31) is canceled out. The same conclusion was also drawn in the recent BHF study of asymmetric NM by Vidaña [41]. Using the single-nucleon potentials given by the present HF calculation, we obtained exactly the same $S(\rho)$ from both Eq. (31) and the expansion (28), neglecting the higher-order terms $O(\delta^3)$ and $O(\delta^4)$, respectively. These results are compared with those given by the general definition (29) in Fig. 8. One can see that the parabolic approximation is reasonable only for $\delta < 1$, and it becomes poorer for pure neutron matter. As a result, the higher-order terms on the right-hand side of Eqs. (28) and (31) need to be taken into account for very neutron-rich matter, as done recently by Chen *et al.* [6].

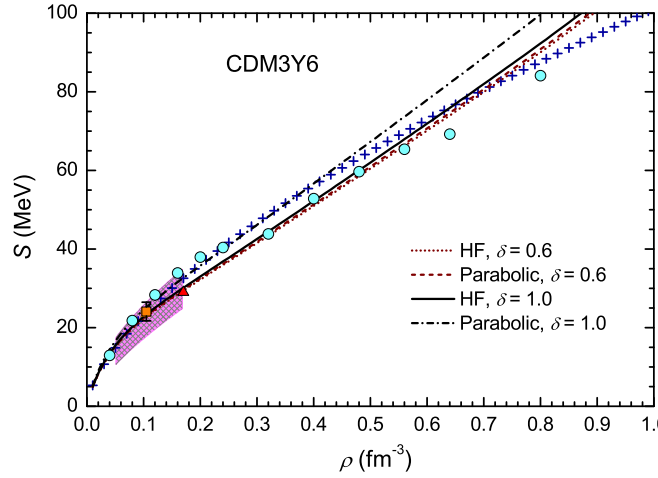

FIG. 8. (Color online) Nuclear symmetry energy $S(\rho)$ at the NP asymmetries $\delta = 0.6$ and 1 obtained with the CDM3Y6 interaction, using the parabolic approximation (28) and general definition (29). The shaded (magenta) region marks the empirical boundaries implied by the analysis of the isospin diffusion data and the double ratio of the neutron and proton spectra observed in the HI collisions [43,45]. The square is the empirical S value implied by the structure study of the GDR [46], and the triangle is that established from the analysis of the terrestrial nuclear physics experiments and astrophysical observations [44]. The circles and crosses are results of the *ab initio* calculations by Akmal *et al.* [47] and Gandolfi *et al.* [48], respectively.

The main method to probe $S(\rho)$ obtained with a chosen in-medium NN interaction is to probe this interaction in the analysis of heavy-ion (HI) collisions [43,45] or in the structure studies of nuclei with large neutron excess [46,49]. Based on the constraints implied by such studies, extrapolation is often made to study the low- and high-density behavior of nuclear symmetry energy. For the illustration, we have compared in Fig. 8 the HF results given by the CDM3Y6 interaction for $S(\rho)$ with the empirical data [43–46,49] and the results of the *ab initio* calculations of the asymmetric NM by Akmal *et al.* [47] and Gandolfi *et al.* [48]. Around the saturation density ρ_0 the symmetry energy S_0 given by the HF calculation is in a very good agreement with the empirical value [44,49]. In the low-density region ($\rho \approx 0.3 \sim 0.6\rho_0$) the empirical boundaries for $S(\rho)$ deduced from the analysis of the isospin diffusion data and double ratio of neutron and proton spectra data of HI collisions [43,45] do enclose our HF result. At the density $\rho \approx 0.1$ fm^{-3}, the HF result also agrees well with the empirical value deduced from the structure study of the giant dipole resonance (GDR) in heavy nuclei [46]. At supranuclear densities, where the reliable empirical data are still absent, our HF results follow closely those of the *ab initio* calculations [47,48].

The explicit contribution of the RT to the nuclear symmetry energy, through the difference between the neutron and proton SP potentials (31), is canceled out. However, the vital role of the rearrangement effects in the HF calculation of the nuclear symmetry energy is well illustrated in Fig. 9, where $S(\rho)$ values

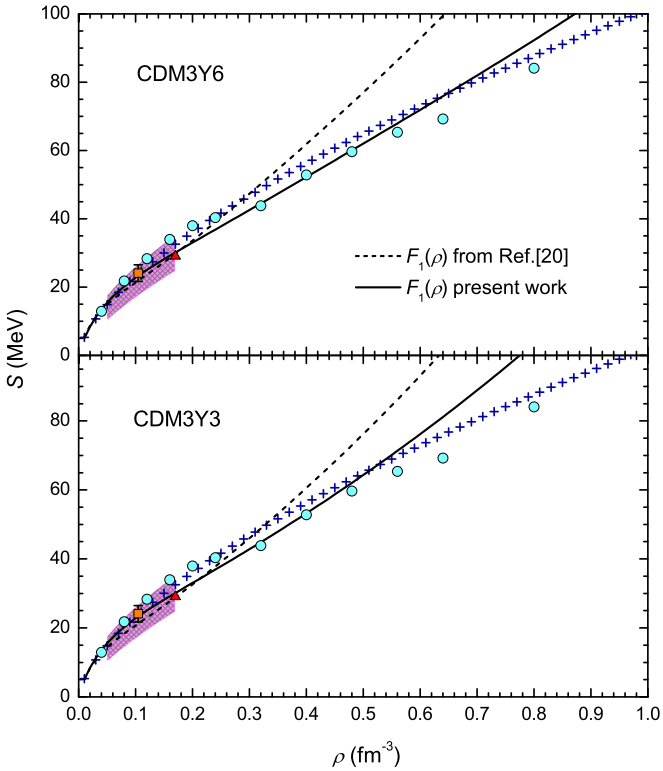

FIG. 9. (Color online) Nuclear symmetry energy $S(\rho)$ given by the HF calculation using the new parameters of the IV density dependence $F_1(\rho)$ of the CDM3Y6 (upper panel) and CDM3Y3 (lower panel) interactions. These same HF results obtained with the old parameters of $F_1(\rho)$ determined in Ref. [20] are shown as the dashed lines. Other symbols are the same as in Fig. 8

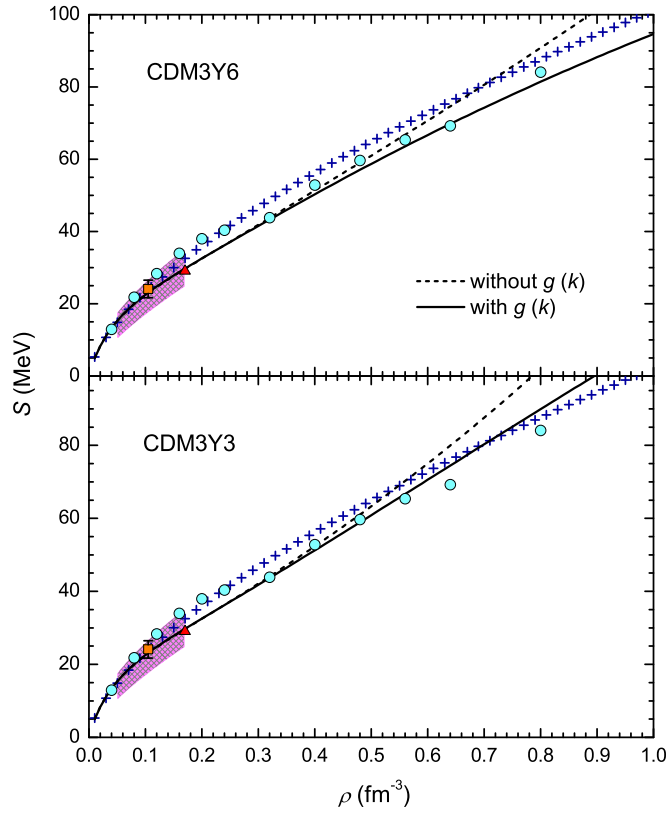

FIG. 10. (Color online) Nuclear symmetry energy $S(\rho)$ obtained at the NP asymmetry $\delta < 1$ from the (HF+RT) SP energies with the CDM3Y6 (upper panel) and CDM3Y3 (lower panel) interactions, using the parabolic approximation (31). The solid (dashed) curves show the results obtained with (without) the modification of the high-momentum part of the SP potential by the $g(k)$ function determined from the observed energy dependence of the nucleon OP. Other symbols are the same as in Fig. 8

obtained from the HF calculation using the new parameters of the IV density dependence $F_1(\rho)$ of the CDM3Yn interactions are compared with those obtained with the old parameters of $F_1(\rho)$, determined in Ref. [20] by fitting the IV part of the (HF only) SP potential to the IV part of the microscopic JLM potential. One can see in Fig. 9 that $S(\rho)$ given by the old IV density dependence agrees with the empirical data and *ab initio* results at NM densities up to about $2\rho_0$ only. Using the new parameters of $F_1(\rho)$ obtained in the present work by fitting the IV part of the (HF+RT) SP potential to the JLM potential (see Fig. 4), the calculated $S(\rho)$ values now follow closely those given by the *ab initio* calculations over a wider range of the NM densities, up to $\rho \approx 4\rho_0$.

With the Fermi momentum k_F becoming larger at high NM densities, a realistic momentum dependence of the SP potentials should be helpful in constraining the nuclear symmetry energy $S(\rho)$ at the supranuclear densities, based on the relation (31). The symmetry energies $S(\rho)$ given by the difference between the neutron- and proton SP energies (31) at the NP asymmetries $\delta < 1$ are shown in Fig. 10, with and without the modification of the high-momentum part of the (HF+RT) nucleon OP by the $g(k_F)$ function determined from the observed energy dependence of the nucleon OP. One can see that the modification of the high-momentum tail of the (HF+RT) SP potential results in a slightly softer slope of the nuclear symmetry energy at the high NM densities that leads, in turn, to a good agreement of the HF results with those of the *ab initio* calculations over a much wider range of the NM density, up to $\rho \approx 5 \sim 6\rho_0$. This result is, thus, complementary to the recent efforts by Li *et al.* [50] to determine the nuclear symmetry from the optical model analysis of the elastic neutron-nucleus scattering over a wide range of energies.

IV. NEUTRON-PROTON EFFECTIVE MASS SPLITTING

As discussed in Sec. II, due to the finite range of the Yukawa functions in the radial part of the CDM3Yn interaction (11), the SP potential depends explicitly on the nucleon momentum k through its exchange term that implies a *nonlocal* single-nucleon potential in the coordinate space. At the high nucleon momenta, the momentum dependence of the SP potential is further modified by the $g(k)$ function implied by the observed energy dependence of the nucleon OP. An important quantity associated with the momentum dependence of the nucleon SP potential is the nucleon effective mass m^*_τ, defined within the

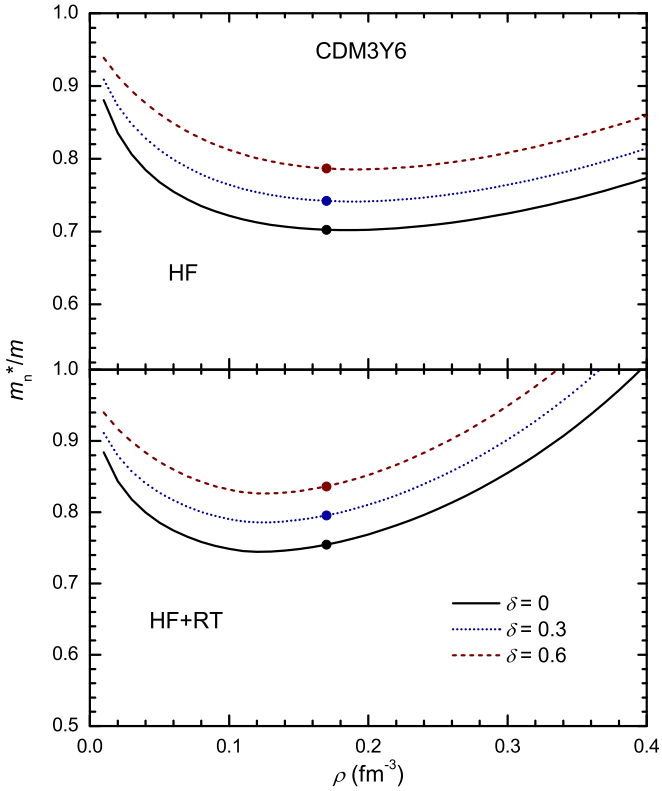

FIG. 11. (Color online) Density dependence of the neutron effective mass (32) at the NP asymmetry $\delta = 0$, 0.3, and 0.6, obtained from the SP potential given by the CDM3Y6 interaction. The HF and HF+RT results are shown in the upper and lower panels, respectively. The solid circles are the effective-mass values determined at the saturation density ρ_0.

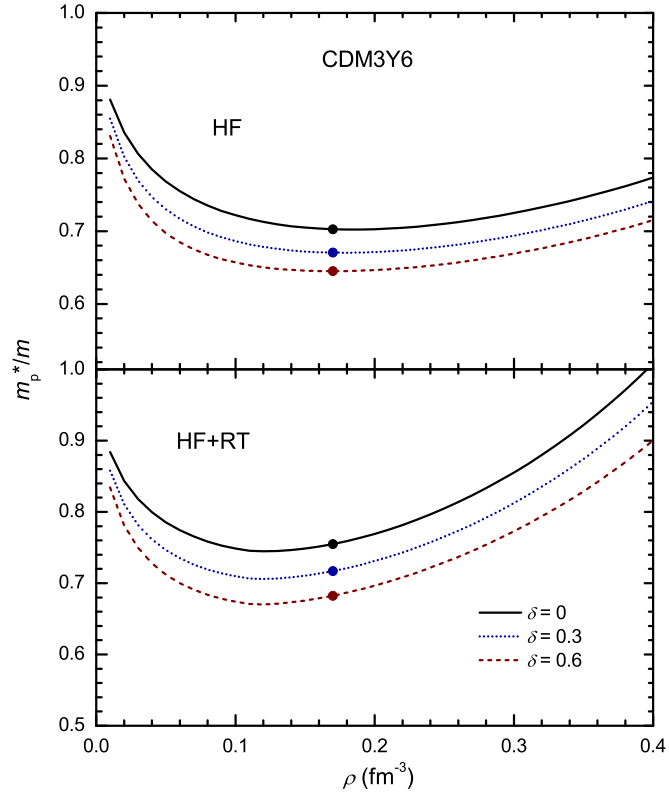

FIG. 12. (Color online) The same as Fig. 11 but for the proton effective mass.

nonrelativistic mean-field formalism as

$$\frac{m_\tau^*(\rho,\delta)}{m} = \left[1 + \frac{m}{\hbar^2 k_F^{(\tau)}} \frac{\partial U_\tau(\rho,\delta,k)}{\partial k}\bigg|_{k_F^{(\tau)}}\right]^{-1}, \qquad (32)$$

where m is the free nucleon mass. Thus, the nucleon effective mass m_τ^* describes the nonlocality of the mean-field potential felt by a nucleon propagating through the nuclear medium. As such, the nucleon effective mass is directly linked to many nuclear physics phenomena, like the dynamics of HI collisions, damping of giant resonances, temperature profile of the hot stellar objects, and neutrino emission therefrom [51]. For the asymmetric NM, the relative difference between the neutron and proton effective masses,

$$m_{n-p}^*(\rho,\delta) = \frac{m_n^*(\rho,\delta) - m_p^*(\rho,\delta)}{m}, \qquad (33)$$

is widely discussed [44,52] as the *neutron-proton effective mass splitting*, which is closely related to the nuclear symmetry energy $S(\rho)$ and its slope parameter L [44]. The NP effective mass splitting was also suggested to affect the neutron-proton ratio during the stellar evolution, and the cooling of protoneutron stars, etc. [52].

In the present work we do not intend to explore this issue over such a wide scope, but focus briefly on the effect of the RT in the determination of the nucleon effective mass within the extended HF formalism as well as the effect caused by the modification of the high-momentum part of the SP potential to match the observed energy dependence of the nucleon OP. The obtained neutron and proton effective masses are shown in Figs. 11 and 12, respectively, and one can see that the RT enhances m_τ^* substantially at high NM densities. A similar behavior of the nucleon effective mass can also be seen in the results of a recent microscopic BHF calculation by Baldo *et al.* [51], where the RT originating from three-body force drastically enhances the nucleon effective mass at the high NM densities (see, e.g., Fig. 1 of Ref. [51]). As found in Sec. III for the nuclear symmetry energy, the modification of the high-momentum part of the (HF+RT) SP potential by the $g(k)$ function implied by the observed energy dependence of the nucleon OP changes slightly the slope of the density dependence of the nucleon effective mass at the high NM densities (see Figs. 13 and 14). Although the nucleon effective mass is still poorly known at the high NM densities and/or the large NP asymmetries, the empirical m^*/m value in the symmetric NM is known to be about 0.73 [53] at the saturation density ρ_0. In good agreement with those empirical data, our HF and HF+RT results obtained with the CDM3Y6 interaction (see Fig. 13) give $m^*/m \approx 0.734$ and 0.755, respectively. The modification of the high-momentum part of the (HF+RT) single-nucleon potential by the $g(k)$ function reduces this result slightly to $m^*/m \approx 0.737$ at $\rho = \rho_0$.

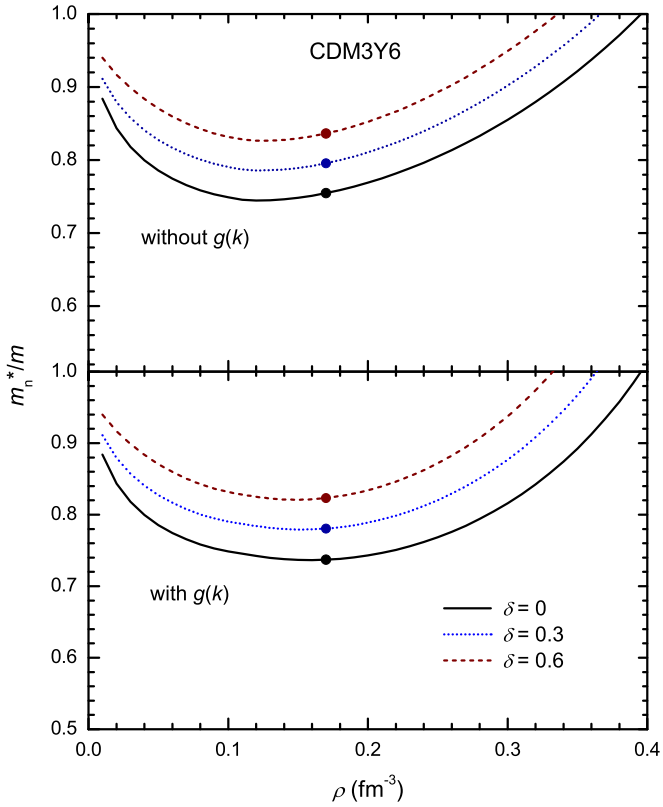

FIG. 13. (Color online) The same (HF+RT) results for the neutron effective mass as in the lower panel of Fig. 11, obtained with (lower panel) or without (upper panel) the modification of the high-momentum part of the SP potential by the $g(k)$ function implied by the observed energy dependence of the nucleon OP.

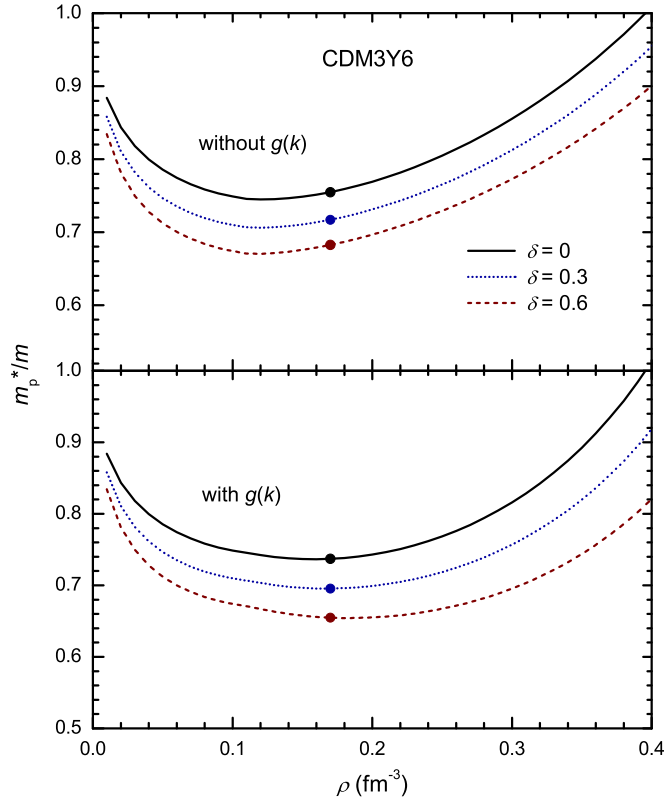

FIG. 14. (Color online) The same as Fig. 13 but for the proton effective mass.

With quite a good agreement of the calculated nucleon effective mass with the empirical data at $\delta = 0$, it is of interest to consider further the δ dependence of the m^*/m value. The HF results obtained at the saturation density ρ_0 are shown in Fig. 15. Given the equal RT contribution to each of the neutron and proton SP potential, the derivative with respect to the nucleon momentum gives about the same RT contribution of around 10% to the neutron and proton effective masses (upper panel of Fig. 15), and the NP effective mass splitting (lower panel of Fig. 15) is rather weakly affected by the rearrangement effect. One can see that both the standard HF and extended HF+RT results show a well defined linear δ dependence of the NP effective mass splitting (33). Our final HF+RT results give $m^*_{n-p}(\rho_0,\delta) \approx (0.26 \pm 0.01)\delta$ which is well inside the empirical boundary $m^*_{n-p}(\rho_0,\delta) \approx (0.27 \pm 0.35)\delta$, established from the analyses of the terrestrial nuclear physics experiments and astrophysical observations [44]. Our result is, however, lower than that estimated recently, $m^*_{n-p}(\rho_0,\delta) \approx (0.41 \pm 0.15)\delta$, from the phenomenological (isospin-dependent) nucleon OP [52] determined from the extensive optical model analysis of a large data set of the nucleon elastic scattering. The uncertainty of 0.01δ in the HF+RT result is *not* statistical error associated with the uncertainties of the model ingredients, but the uncertainty in adopting a linear δ dependence of the NP effective mass splitting (33) in Fig. 15. This fact indicates simply that at $\delta < 1$, when the parabolic approximation (28) and (31) is reasonable for the nuclear symmetry energy, the first-order symmetry term in the expansion of the single-nucleon potential over δ (see, e.g., Ref. [6]) contributes overwhelmingly to the determination of the $m^*_{n-p}(\rho,\delta)$ value.

With larger Fermi momentum k_F at the high NM densities, the modification of the momentum dependence of the SP potentials by the $g(k_F)$ function determined from the observed energy dependence of the nucleon OP should be taken into account in the HF+RT calculation of the NP effective mass splitting. One can see in Fig. 16 that $m^*_{n-p}(\rho,\delta)$ becomes larger at $\rho = 2\rho_0$, and is enhanced further by more than 50% when the modification of the high-momentum part of the SP potential is taken into account. The behavior of the nucleon effective mass (32) and the NP effective mass splitting (33) at the supranuclear densities is still poorly known, and the difference in the HF+RT results for the NP effective mass splitting, $m^*_{n-p}(\rho,\delta) \approx (0.48 \pm 0.01)\delta$ at $\rho = 2\rho_0$ compared to $(0.26 \pm 0.01)\delta$ at $\rho = \rho_0$, is quite significant and should be of interest for the nuclear astrophysical studies.

V. FOLDING MODEL OF THE NUCLEON OPTICAL POTENTIAL

Given the substantial rearrangement effects to the nucleon OP found above in the extended HF calculation of the NM, it is of high interest to study these effects in the many-body calculation of the nucleon OP of the finite nuclei. As such, the folding model (more precisely the single-folding model)

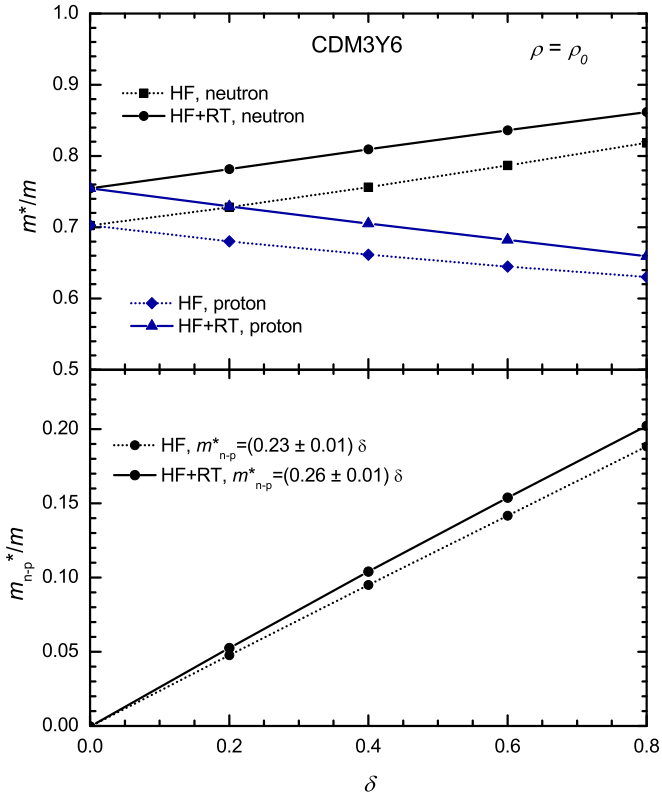

FIG. 15. (Color online) Neutron and proton effective masses (upper panel) and their splitting (lower panel) obtained at $\rho = \rho_0$ and the different NP asymmetries δ. Both the HF and HF+RT results show a well defined linear δ dependence of the NP effective mass splitting (33).

has been proven to be a very effective tool to estimate the nucleon OP [19,54,55]. It can be seen from the basic folding formulas that this model generates the first-order term of the

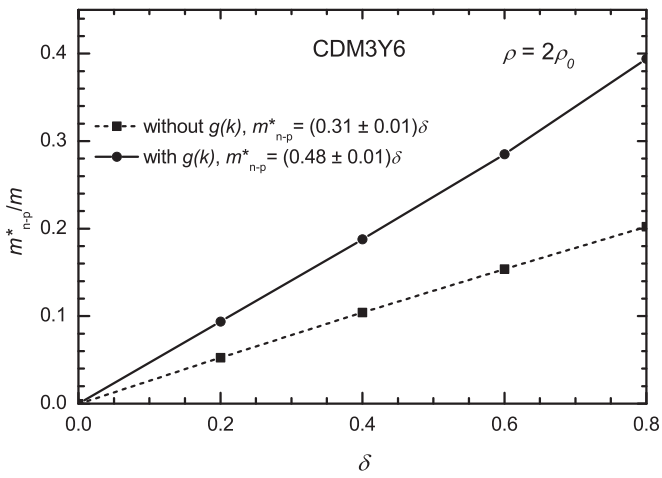

FIG. 16. δ dependence of the neutron-proton effective mass splitting obtained at $\rho = 2\rho_0$. The HF+RT results were obtained with (solid line) or without (dashed line) the modification of the high-momentum part of the SP potential by the $g(k)$ function determined from the observed energy dependence of the nucleon OP.

microscopic OP defined in Feshbach's formalism of nuclear reactions [56], based on the nucleon degrees of freedom. The success of the single-folding approach in the description of the elastic nucleon-nucleus scattering data measured for the targets in the different mass regions suggests that the first-order term of the Feshbach's microscopic OP is indeed the dominant part of the nucleon OP.

In the single-folding approach, the central OP of the τ-kind nucleon incident on the target A at the energy E is evaluated as a HF-type potential [19], using an appropriate, energy and density dependent effective NN interaction $v_c(\rho, E)$,

$$\begin{aligned} U_\tau^{\rm HF}(E,R) &= \sum_{j\in A}\big[\langle \boldsymbol{k}_\tau, j|v_c^{\rm D}(\rho,E)|\boldsymbol{k}_\tau, j\rangle \\ &\quad + \langle \boldsymbol{k}_\tau, j|v_c^{\rm EX}(\rho,E)|j,\boldsymbol{k}_\tau\rangle\big], \\ &= \sum_{j\in A}\langle \boldsymbol{k}_\tau, j|v_c(\rho,E)|\boldsymbol{k}_\tau, j\rangle_{\mathcal{A}}, \end{aligned} \tag{34}$$

where $|j\rangle$ is the single-nucleon wave function of the jth nucleon of the target. The antisymmetrization $\mathcal{A}$ of the nucleon-nucleus system is done by taking into account explicitly the knock-on exchange effects. As a result, the exchange term of U_τ becomes nonlocal in the coordinate space [55]. An accurate local approximation is usually made by treating the relative motion locally as a plane wave [19,54], and the *local* energy dependent folded potential (34) is obtained as an explicit function of the nucleon-nucleus distance R and local momentum $k(R)$ of the incident nucleon.

At the low incident energies, the pair-wise interaction between the incident nucleon and the nucleons bound in the target can induce certain rearrangement of the SP configurations of the target nucleons that can be observed experimentally in the nucleon removal reactions [35]. In terms of the nucleon-nucleus interaction, such a rearrangement effect is expected to affect also the shape and strength of the nucleon-nucleus OP (34), constructed in the folding model on the HF level from the SP wave functions of the target nucleons. On the other hand, if we make a *local density approximation* (LDA) for the SP potential (20) by replacing the plane waves $|\boldsymbol{k}'\sigma'\tau'\rangle$ by the SP wave functions $|j\rangle$ of the target nucleons, then the resulted potential is just the HF-type folded potential (34) added by a rearrangement term, through the contribution of the Δv_c term. Thus, the total (central) nucleon OP now becomes

$$\begin{aligned} U_\tau(E,R) &= U_\tau^{\rm HF}(E,R) + U_\tau^{\rm RT}(E,R) \\ &= \sum_{j\in A}\langle \boldsymbol{k}_\tau, j|v_c(\rho,E) + \Delta v_c(\rho)|\boldsymbol{k}_\tau, j\rangle_{\mathcal{A}}, \end{aligned} \tag{35}$$

with $U^{\rm RT}$ originating from the explicit density dependence of the CDM3Yn interaction (11). In the standard HF formalism for the nucleon mean-field potential, the HF potential for an unbound (scattering) nucleon has been assumed years ago [57,58] as the first-order term of the microscopic OP for the low-energy elastic nucleon scattering, in about the same scheme as that of the Feshbach's microscopic OP [56]. Applying the variational HF method to obtain the scattering equation for the nucleon-nucleus system, a rearrangement contribution to the HF potential appears naturally if the

effective NN interaction is density dependent [59]. Given the rearrangement contribution to the density dependence of the CDM3Yn interaction determined above in the HF study of the NM, it is now possible to consistently include the RT into the folding calculation of the nucleon-nucleus potential (34).

Making explicit the neutron and proton SP wave functions in Eq. (35) and using the same isospin-dependent CDM3Yn interactions (11), we obtain the real nucleon OP explicitly in terms of the (energy dependent) isoscalar and isovector parts as

$$U_\tau(E,R) = U_{\rm IS}(E,R) \pm U_{\rm IV}(E,R), \tag{36}$$

where the $(-)$ sign pertains to the proton OP and the $(+)$ sign to the neutron OP,

$$\begin{aligned} U_{\rm IS}(E,R) = g(k(E,R)) \int [F_0(\rho(\boldsymbol{r})) + \Delta F_0(\rho(\boldsymbol{r}))] \\ \times \big\{[\rho_n(\boldsymbol{r}) + \rho_p(\boldsymbol{r})] v_{00}^{\rm D}(s) + [\rho_n(\boldsymbol{R},\boldsymbol{r}) \\ + \rho_p(\boldsymbol{R},\boldsymbol{r})] v_{00}^{\rm EX}(s) j_0(k(E,R)s)\big\} d^3r, \end{aligned} \tag{37}$$

$$\begin{aligned} U_{\rm IV}(E,R) = g(k(E,R)) \int [F_1(\rho(\boldsymbol{r})) + \Delta F_1(\rho(\boldsymbol{r}),T_z(\boldsymbol{r}))] \\ \times \big\{[\rho_n(\boldsymbol{r}) - \rho_p(\boldsymbol{r})] v_{01}^{\rm D}(s) + [\rho_n(\boldsymbol{R},\boldsymbol{r}) \\ - \rho_p(\boldsymbol{R},\boldsymbol{r})] v_{01}^{\rm EX}(s) j_0(k(E,R)s)\big\} d^3r. \end{aligned} \tag{38}$$

Here, $\rho_\tau(\boldsymbol{r},\boldsymbol{r}')$ is the nonlocal SP density matrix of the target with $\rho_\tau(\boldsymbol{r}) \equiv \rho_\tau(\boldsymbol{r},\boldsymbol{r})$, and $k(E,R)$ is the local momentum of the incident nucleon determined self-consistently from the total real nucleon OP as

$$k(E,R) = \sqrt{\frac{2\mu}{\hbar^2}[E_{\rm c.m.} - U_\tau(E,R)]}. \tag{39}$$

Similarly to the expression of the nucleon OP in the NM limit (27), the folded nucleon-nucleus potential (36) also depends explicitly on the momentum (39) of the incident nucleon through the (*localized*) exchange term. To estimate properly the contribution of the rearrangement effects, the IS and IV density dependencies of the RT in Eqs. (37) and (38) are determined in the LDA from the $\Delta F_0(\rho)$ and $\Delta F_1(\rho,\delta)$ values given by the HF study of the NM (18), accurately interpolated for the local nuclear density $\rho = \rho(\boldsymbol{r}) = \rho_n(\boldsymbol{r}) + \rho_p(\boldsymbol{r})$ and the neutron-proton asymmetry $\delta = T_z(\boldsymbol{r}) = [\rho_n(\boldsymbol{r}) - \rho_p(\boldsymbol{r})]/\rho(\boldsymbol{r})$.

It can be seen from Eqs. (37) and (38) that the energy dependence of the real nucleon OP (36) is determined entirely by the local momentum of the incident nucleon $k(E,R)$ appearing in the exchange potential as well as in the $g(k(E,R))$ function. Given the $g(k)$ function determined above in the HF study of the NM based on the observed energy dependence of the nucleon OP, each local scaling factor $g(k(E,R))$ of the folded potential is interpolated from the $g(k)$ function (see Fig. 3) at the local momentum $k = k(E,R)$. As a result, $g(k(E,R))$ can now be considered as the explicit energy (or momentum) dependence of the density dependent CDM3Yn interaction (11), locally consistent with the nucleon mean-field potential (36). This is an essential improvement of the present formulation of the single-folding model, compared to the earlier applications of the folding model (see, e.g., Ref. [19]) where a constant factor $g(E) \approx 1 - 0.0026E$ was used to scale the CDM3Y6 interaction. Because of the self-consistent determination of the $g(k(E,R))$ function and contribution of the RT through $\Delta F_0(\rho(\boldsymbol{r}))$ and $\Delta F_1(\rho(\boldsymbol{r}),T_z(\boldsymbol{r}))$, the single-folding calculation (37) and (38) becomes more cumbersome and time consuming compared with the earlier version [19] of the folding model.

Although a comprehensive folding model study of the elastic nucleon-nucleus scattering based on the new formulation of the model should be the subject of a separate study, we have considered selectively in the present work the data of the elastic neutron scattering on the lead target, measured at the incident energies of 30.4 and 40 MeV [29]. Given no Coulomb interference and the energies close to the Fermi energy ($E_F \approx 38.7$ MeV obtained with the Fermi momentum $k_F \approx 1.36\,{\rm fm}^{-1}$), the considered elastic neutron scattering data should be a good test ground for the improved single-folding approach suggested in the present work, with the rearrangement effects consistently taken into account. For the ^{208}Pb target we have used the empirical neutron and proton densities deduced from the high-precision elastic proton scattering at 800 MeV by Ray *et al.* [60,61]. These densities are available in the analytical form, and they have been used recently in our folding model analysis [62] of the charge-exchange (^{3}He,t) scattering to the isobar analog state of the target, to determine the thickness of the neutron skin in ^{208}Pb.

From the folded $n + ^{208}$Pb potentials shown in Fig. 17 one can see that the standard folding method [19] gives a rather deep HF-type folded potential. After the RT is taken properly into account, the HF+RT folded potential becomes substantially shallower, much closer to the empirical Woods-Saxon potential given by the global CH89 parametrizations of the nucleon OP [38], which was proven to be accurate for the elastic nucleon scattering from medium and heavy targets at the incident energies below 100 MeV. The agreement of the HF+RT folded potential with the empirical CH89 potential becomes better, especially at the neutron energy of 40 MeV, when the scaling $g(k(E,R))$ function is consistently taken into account. To further test the folded $n + ^{208}$Pb potentials shown in Fig. 17, they were used (without any further renormalization of their strength) as the real OP in the standard optical model (OM) calculation of the elastic $n + ^{208}$Pb scattering at 30.4 and 40 MeV using the code ECIS06 written by Raynal [63], with the imaginary and spin-orbital parts of the OP taken from the global systematics CH89 [38]. From the comparison of the calculated cross sections with the measured data [29] in Fig. 18 one can see that a very good OM description of the data has been obtained with the real folded OP after the RT is included. Although the OM fit is marginally improved after the HF+RT folded potential is scaled with the scaling function $g(k(E,R))$, it is important to note that this scaling function is resulted from the realistic momentum dependence of the SP potential in the NM discussed in Sec. II. The local momentum $k(E,R)$ of the incident neutron is largest in the center, and approaches its asymptotic value at the potential surface (determined for a free neutron whose kinetic energy is equal the incident energy)

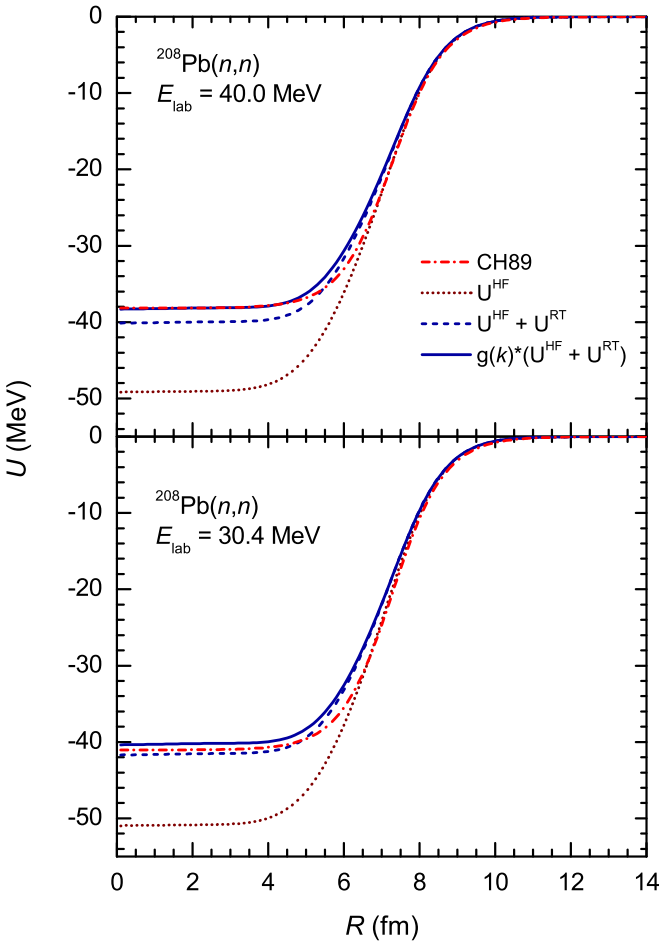

FIG. 17. (Color online) Real $n+^{208}$Pb optical potential at the neutron incident energies of 30.4 and 40 MeV predicted by the single-folding calculation (37) and (38) using the CDM3Y6 interaction, with and without the contributions of the RT and the scaling $g(k(E,R))$ function. CH89 is the phenomenological OP taken from the global systematics by Varner *et al.* [38].

(see upper panel of Fig. 19). As a result, the $g(k(E,R))$ value is ranging smoothly from about 0.96 at small radii to unity at the potential surface, which is a rather mild mean-field effect on the shape of the folded nucleon-nucleus potential. In any case, such a scaling function is physically much more consistent compared to a constant $g(E)$ factor used in the earlier version of the folding model [19] at each nucleon incident energy. The standard HF folded potential is too deep in the center and cannot deliver a good OM description of the data (see Fig. 18) unless its strength is *renormalized* by a factor $N_R \approx 0.85$. A renormalization factor $N_R < 1$ of the real folded OP was often obtained in the earlier folding model analyses of the elastic nucleon scattering [20], and the lack of the contribution from the RT is likely the main reason.

With a very good OM description of the considered elastic neutron scattering data by the HF+RT folded potential, the reliability of the folding model in predicting the nucleon-nucleus OP seems much improved. In view of the new folding formalism suggested in the present work, a systematic folding model analysis of the elastic and inelastic nucleon-nucleus

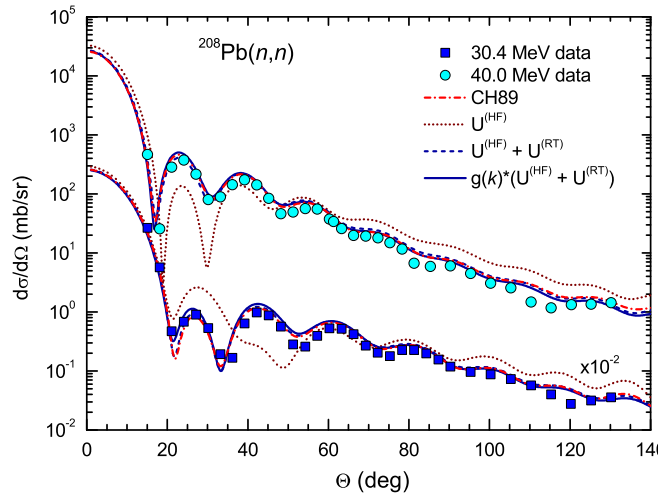

FIG. 18. (Color online) Elastic $n+^{208}$Pb scattering cross sections at the neutron incident energies of 30.4 and 40 MeV obtained with the real OP's shown in Fig. 17, in comparison with the data measured by DeVito *et al.* [29]. The imaginary and spin-orbital parts of the OP taken from the global systematics CH89 [38] were used in the OM calculation.

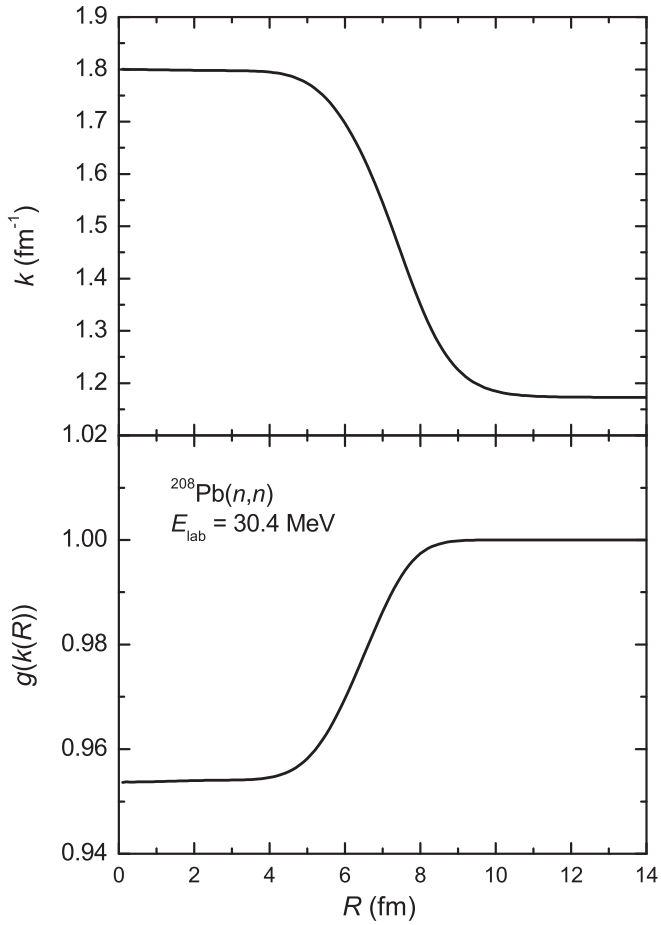

FIG. 19. Local momentum $k(E,R)$ of the incident neutron (upper panel) and the scaling function $g(k(E,R))$ (lower panel) determined self-consistently from the HF+RT real folded $n+^{208}$Pb potential obtained with the CDM3Y6 interaction at the neutron energy $E =$ 30.4 MeV.

scattering over a wide range of energies should be of high interest.

VI. SUMMARY

A consistent HF study of the asymmetric NM has been done using the CDM3Y3 and CDM3Y6 density dependent versions of the M3Y-Paris interaction, with the focus on the rearrangement term of the SP potential that arises naturally when the Hugenholtz–Van Hove theorem is applied to calculate SP energy from the total NM energy. Based on the exact expression of the RT of the isospin dependent SP potential given by the HVH theorem at each NM density and the empirical energy dependence of the nucleon OP observed over a wide range of energies, a simple method has been proposed to account effectively for the momentum dependence of the RT of the SP potential in the standard HF scheme, with an explicit contribution of the RT added to the density dependence of the CDM3Yn interaction (11). The HF+RT SP potentials obtained at the different NM densities and neutron-proton asymmetries agree reasonably with those predicted by the microscopic BHF calculations of the NM that have the higher-order rearrangement term properly included [3,41].

Given a direct link between the SP potential in the NM and the nuclear symmetry [4,7], we have determined anew the parameters of the isovector density dependence of the CDM3Yn interaction (11) by matching our HF+RT results for the IV part of the nucleon OP in the NM with those of the BHF calculation by the JLM group [31,32]. Using these new parameters, the calculated nuclear symmetry energy $S(\rho)$ agrees nicely with the latest empirical constraints at $\rho \leqslant \rho_0$ as well as the results of the *ab initio* calculations of the asymmetric NM at $\rho > \rho_0$. With the high-momentum part of the SP potential modified based on the observed energy dependence of the nucleon OP, the nuclear symmetry energy $S(\rho)$ obtained in the parabolic approximation from the difference between the neutron and proton SP energies turns out to be in very good agreement with that given by the *ab initio* calculations over a wide range of the NM densities. This result indicates that one might indirectly learn about the density dependence of the nuclear symmetry energy from the extensive OM studies of the elastic nucleon-nucleus scattering at low, medium, and intermediate energies.

The momentum dependence of the SP potential obtained in the HF+RT calculation has a very well defined linear δ dependence of the NP effective mass splitting (33), with $m^*_{n-p}(\rho_0,\delta) \approx (0.26 \pm 0.01)\delta$ that agrees well with the empirical constraint from the recent analysis of the terrestrial nuclear physics experiments and astrophysical observations [44]. The $m^*_{n-p}(\rho,\delta)$ value was found to be readily increased with the increasing NM density up to $2\rho_0$, while retaining its linear δ dependence. Although there is no empirical constraint for the NP effective mass splitting at the high NM densities to compare with, we have shown here that a proper treatment of the RT and a realistic momentum dependence of the single-nucleon potential are prerequisites for the determination of $m^*_{n-p}(\rho,\delta)$ at the different NM densities that can be of interest for the nuclear astrophysical studies.

A very important milestone of the present work is that the proper treatment of the rearrangement effects and momentum dependence of the nucleon mean-field potential in the HF calculation of the NM has led us to the important physics inputs that enable a consistent inclusion of the RT into the HF-type folding model calculation of the nucleon OP of the finite nuclei in the same mean-field manner. The contribution of the RT has been shown, in an application of the extended folding model to study the elastic $n + {}^{208}$Pb scattering, to be vital in obtaining the realistic shape and strength of the real nucleon OP. The predicting power of the folding model for the nucleon OP seems much improved. A systematic folding model analysis of the elastic and inelastic nucleon-nucleus scattering over a wide range of energies is now planned with the extended folding formalism.

ACKNOWLEDGMENTS

We thank B. A. Li and C. Xu for their helpful communications. The present research has been supported by the National Foundation for Scientific and Technological Development (NAFOSTED Project No. 103.04-2014.76).

[1] C. Mahaux, P. F. Bortignon, R. A. Broglia, and C. H. Dasso, Phys. Rep. **120**, 1 (1985).
[2] I. Bombaci and U. Lombardo, Phys. Rev. C **44**, 1892 (1991).
[3] W. Zuo, I. Bombaci, and U. Lombardo, Phys. Rev. C **60**, 024605 (1999).
[4] W. Zuo, I. Bombaci, and U. Lombardo, Eur. Phys. J. A **50**, 12 (2014).
[5] C. Xu, B. A. Li, and L. W. Chen, Phys. Rev. C **82**, 054607 (2010).
[6] R. Chen, B. J. Cai, L. W. Chen, B. A. Li, X. H. Li, and C. Xu, Phys. Rev. C **85**, 024305 (2012).
[7] C. Xu, B. A. Li, and L. W. Chen, Eur. Phys. J. A **50**, 21 (2014).
[8] C. J. Horowitz, E. F. Brown, Y. Kim, W. G. Lynch, R. Michaels, A. Ono, J. Piekarewicz, M. B. Tsang, and H. H. Wolter, J. Phys. G **41**, 093001 (2014).
[9] B. A. Li, L. W. Chen, and C. M. Ko, Phys. Rep. **464**, 113 (2008).
[10] M. Baldo and C. Maieron, J. Phys. G **34**, R243 (2007).
[11] G. Bertsch, J. Borysowicz, H. McManus, and W. G. Love, Nucl. Phys. A **284**, 399 (1977).
[12] N. Anantaraman, H. Toki, and G. F. Bertsch, Nucl. Phys. A **398**, 269 (1983).
[13] D. T. Khoa and W. von Oertzen, Phys. Lett. **B304**, 8 (1993).
[14] D. T. Khoa and W. von Oertzen, Phys. Lett. **B342**, 6 (1995).
[15] D. T. Khoa, W. von Oertzen, and A. A. Ogloblin, Nucl. Phys. A **602**, 98 (1996).
[16] H. S. Than, D. T. Khoa, and N. V. Giai, Phys. Rev. C **80**, 064312 (2009).
[17] D. T. Loan, N. H. Tan, D. T. Khoa, and J. Margueron, Phys. Rev. C **83**, 065809 (2011).

[18] D. T. Khoa, G. R. Satchler, and W. von Oertzen, Phys. Rev. C **56**, 954 (1997).
[19] D. T. Khoa, E. Khan, G. Colò, and N. V. Giai, Nucl. Phys. A **706**, 61 (2002).
[20] D. T. Khoa, H. S. Than, and D. C. Cuong, Phys. Rev. C **76**, 014603 (2007).
[21] D. T. Khoa, W. von Oertzen, H. G. Bohlen, and S. Ohkubo, J. Phys. **G34**, R111 (2007).
[22] N. D. Chien and D. T. Khoa, Phys. Rev. C **79**, 034314 (2009).
[23] D. T. Khoa, B. M. Loc, and D. N. Thang, Eur. Phys. J. A **50**, 34 (2014).
[24] D. T. Khoa, G. R. Satchler, and W. von Oertzen, Phys. Rev. C **51**, 2069 (1995).
[25] G. E. Brown, Rev. Mod. Phys. **43**, 1 (1971).
[26] A. B. Migdal, *Theory of Finite Fermi Systems and Applications to Atomic Nuclei* (Interscience, New York, 1967).
[27] N. M. Hugenholtz and L. Van Hove, Physica **24**, 363 (1958).
[28] P. Czerski, A. De Pace, and A. Molinari, Phys. Rev. C **65**, 044317 (2002).
[29] R. P. DeVito, D. T. Khoa, S. M. Austin, U. E. P. Berg, and B. M. Loc, Phys. Rev. C **85**, 024619 (2012).
[30] L. Satpathy, V. S. Uma Maheswari, R. C. Nayak, Phys. Rep. **319**, 85 (1999).
[31] J. P. Jeukenne, A. Lejeune, and C. Mahaux, Phys. Rev. C **16**, 80 (1977).
[32] A. Lejeune, Phys. Rev. C **21**, 1107 (1980).
[33] A. M. Lane, Phys. Rev. Lett. **8**, 171 (1962).
[34] G. R. Satchler, *Isospin in Nuclear Physics*, edited by D. H. Wilkinson (North-Holland, Amsterdam, 1969), p. 390.
[35] P. E. Hodgson, Rep. Prog. Phys. **38**, 847 (1975).
[36] C. Mahaux and R. Sartor, Adv. Nucl. Phys. **20**, 1 (1991).
[37] A. Bohr and B. R. Mottelson, *Nuclear Structure* (W. A. Benjamin, Inc., New York, 1969), Vol. I, p. 237.
[38] R. L. Varner, W. J. Thompson, T. L. McAbee, E. J. Ludwig, and T. B. Clegg, Phys. Rep. **201**, 57 (1991).
[39] S. Hama, B. C. Clark, E. D. Cooper, H. S. Sherif, and R. L. Mercer, Phys. Rev. C **41**, 2737 (1990).
[40] J. P. Jeukenne, A. Lejeune, and C. Mahaux, Phys. Rev. C **15**, 10 (1977).
[41] I. Vidaña, *Tensor Force, Rearrangement & Symmetry Energy*, Talk given at 3rd International Symposium on Nuclear Symmetry Energy, NSCL/FRIB, East Lansing, July, (2013); http://www.nucl.phys.tohoku.ac.jp/nusym13/program.html.
[42] R. B. Wiringa, V. G. J. Stoks, and R. Schiavilla, Phys. Rev. C **51**, 38 (1995).
[43] M. B. Tsang, Y. Zhang, P. Danielewicz, M. Famiano, Z. Li, W. G. Lynch, and A. W. Steiner, Phys. Rev. Lett. **102**, 122701 (2009).
[44] B. A. Li and X. Han, Phys. Lett. **B727**, 276 (2013).
[45] A. Ono, P. Danielewicz, W. A. Friedman, W. G. Lynch, and M. B. Tsang, Phys. Rev. C **68**, 051601(R) (2003).
[46] L. Trippa, G. Colò, and E. Vigezzi, Phys. Rev. C **77**, 061304(R) (2008).
[47] A. Akmal, V. R. Pandharipande, and D. G. Ravenhall, Phys. Rev. C **58**, 1804 (1998).
[48] S. Gandolfi, A. Yu. Illarionov, S. Fantoni, J. C. Miller, F. Pederiva, and K. E. Schmidt, Mon. Not. R. Astron. Soc. **404**, L35 (2010).
[49] R. J. Furnstahl, Nucl. Phys. A **706**, 85 (2002).
[50] X. H. Li, B. J. Cai, L. W. Chen, R. Chen, B. A. Li, and C. Xu, Phys. Lett. **B721**, 101 (2013).
[51] M. Baldo, G. F. Burgio, H. J. Schulze, and G. Taranto, Phys. Rev. C **89**, 048801 (2014).
[52] B. A. Li and L. W. Chen, Mod. Phys. Lett. A **30**, 1530010 (2015).
[53] P. E. Hodgson, Contemp. Phys. **24**, 491 (1983).
[54] F. A. Brieva and J. R. Rook, Nucl. Phys. A **307**, 493 (1978).
[55] K. Amos, P. J. Dortmans, S. Karataglidis, H. V. von Geramb, and J. Raynal, Adv. Nucl. Phys. **25**, 275 (2001).
[56] H. Feshbach, *Theoretical Nuclear Physics* (Wiley, New York, 1992), Vol. II.
[57] N. Vinh Mau and A. Bouyssy, Nucl. Phys. A **257**, 189 (1976).
[58] V. Bernard and N. V. Giai, Nucl. Phys. A **327**, 397 (1979).
[59] H. Nakada and T. Shinkai, arXiv:nucl-th/0608012.
[60] L. Ray, G. W. Hoffmann, G. S. Blanpied, W. R. Coker, and R. P. Liljestrand, Phys. Rev. C **18**, 1756 (1978).
[61] L. Ray, W. R. Coker, and G. W. Hoffmann, Phys. Rev. C **18**, 2641 (1978).
[62] B. M. Loc, D. T. Khoa, and R. G. T. Zegers, Phys. Rev. C **89**, 024317 (2014).
[63] J. Raynal, *Computing as a Language of Physics* (IAEA, Vienna, 1972), p. 75; coupled-channel code ECIS06 (unpublished).